Available online at www.sciencedirect.com
ScienceDirect
Coordination Chemistry Reviews 252 (2008) 273–295
COORDINATION CHEMISTRY REVIEWS
www.elsevier.com/locate/ccr

Review

The manganese complex of photosystem II in its reaction cycle—Basic framework and possible realization at the atomic level

Holger Dau *, Michael Haumann *

Freie Universität Berlin, FB Physik, Arnimallee 14, D-14195 Berlin, Germany

Received 24 March 2007; accepted 1 September 2007
Available online 6 September 2007

Contents

Abstract

Photosynthetic water oxidation proceeds at a pentanuclear Mn_4Ca complex bound to amino acid residues in the interior of photosystem II (PSII). It involves the binding of two water molecules, the removal of four electrons and four protons from the Mn-complex/substrate-water entity, O–O bond formation, and dioxygen release. Basic aspects of the reaction cycle of the Mn complex of PSII are discussed: (1) Kok's classical S-state cycle

Abbreviations: EPR, electron paramagnetic resonance (spectroscopy); E_c, configurational potential of the elementary redox reaction; E_m, redox potential (versus normal hydrogen electrode); ET, electron transfer; FTIR, Fourier-transform infrared (spectroscopy); EXAFS, extended X-ray absorption fine-structure; PSII, photosystem II; P680, primary chlorophyll donor; RIXS, resonant inelastic X-ray scattering; UV/vis, spectroscopy in the ultra-violet and visible range; XANES, X-ray absorption near-edge structure; XAS, X-ray absorption spectroscopy; Y_Z, Tyr_{160} or Tyr_{161} (species-dependent) of the D1 protein of PSII.

* Corresponding authors. Tel.: +49 30 838 53581; fax: +49 30 838 56299.
E-mail addresses: holger.dau@physik.fu-berlin.de (H. Dau), haumann@physik.fu-berlin.de (M. Haumann).

doi:10.1016/j.ccr.2007.09.001

and the corresponding experimental paradigm; (2) recent observations on the (still) enigmatic S_4 state; (3) sequence and characteristics of electron transfer and proton release; (4) a basic nine-step reaction cycle involving eight steps of alternating deprotonation and oxidation of the Mn-complex prior to O–O bond formation and dioxygen release; (5) the energetic constraints of water oxidation in PSII and their mechanistic consequences. In the second part it is considered how the suggested nine-step reaction cycle possibly is realized at the atomic level: (i) studies on synthetic Mn complexes suggest that deprotonation of μ-hydroxo bridges or formation of new μ-oxo bridges could facilitate successive oxidation steps without prohibitive potential increase. (ii) Current structural models of the PSII Mn complex derived from X-ray absorption spectroscopy and/or protein crystallography are discussed. (iii) Structural and oxidation-state changes of the Mn complex are related to the basic nine-step reaction cycle. (iv) As a framework for mechanistic models at the atomic level, we propose that water is oxidized only after the accumulation of four bases which function as proton acceptors in the dioxygen formation step.

Keywords: Manganese complex; Catalytic cycle; Oxygen evolution; Photosynthesis; Water oxidation; X-ray absorption spectroscopy

1. Introduction

Driven by the absorption of four photons, plants and cyanobacteria oxidize water, thereby producing the atmospheric dioxygen [1–8]. Water oxidation by photosystem II (PSII) is of fundamental importance for atmosphere (O_2 production) and biosphere (primary biomass formation). Development of biotechnological and biomimetic approaches for light-driven H_2-production from water could contribute to the worldwide endeavor of moving from fossil fuels to hydrogen-based fuel technologies [9–13]. In this realm, elucidation of the mechanism of photosynthetic water oxidation by PSII is of prime interest—including the light-driven assembly of the Mn_4Ca complex [14–16], light adaptation, photodestruction, photoprotection, and repair mechanisms [17–22].

The catalyst of water splitting is a pentanuclear Mn_4Ca complex (in the following denoted as Mn complex) bound to the proteins of photosystem II (PSII); it functions in concord with a nearby tyrosine residue, the Tyr_{160} or Tyr_{161} of the D1 protein (in the following denoted as Y_Z) [1–6]. In PSII, light absorption is followed by electron transfer from the primary chlorophyll donor (P680) via a specific pheophytin to a firmly bound plastoquinone (Q_A) and subsequently to the secondary quinone acceptor (Q_B) which, when doubly reduced and protonated, can leave its binding site (Fig. 1). At the donor side of PSII, Y_Z is oxidized by $P680^+$ before the Mn complex advances in its water-oxidation cycle. This catalytic cycle is the central subject of the here presented review.

The crystallographic models of PSII [23–27] have revealed an array of numerous cofactors and protein subunits which is both, awe-inspiring and bewildering. On the basis of results obtained in the past three decades of photosynthesis research, a distinct function could be assigned to most of the cofactors resolved in the crystallographic model. The PSII model presented in 2001 by Berlin researchers revealed the position of the Mn complex [23]. Barber and coworkers in London presented a first detailed model of the manganese complex and its ligand environment in 2004 [25]. They could show that the manganese complex includes a Ca ion and thus is a pentanuclear Mn_4Ca complex, in agreement with earlier EXAFS results [28–31]. In 2005, at an improved resolution of 3 Å, the Berlin researchers proposed a model [26] which deviates from the London model [25] with respect to some of the amino acid residues ligating the metal ions of the Mn complex. In all crystallographic data, the putative chloride cofactor

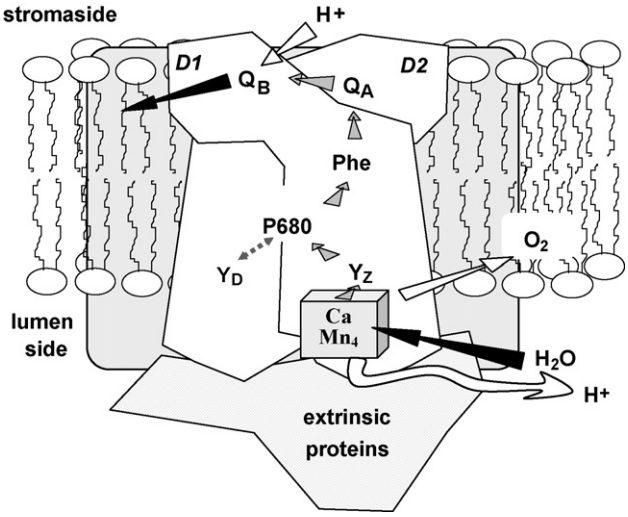

Fig. 1. Arrangement of essential cofactors in photosystem II (PSII). The PSII is embedded in the thylakoid membrane separating the inner-thylakoid lumen from the stroma. Water oxidation involves proton release into the inner-thylakoid compartment, which in the main body of the text often is denoted as lumenal bulk phase.

[32–35] has not been resolved. Presumably the chloride is not a first-sphere Mn–ligand, at least in the dark-adapted PSII [36].

We note that a definitive structural model of the Mn_4Ca complex can not be concluded from the crystallographic data alone, inter alia because of Mn reduction by X-ray exposure during data collection [26,37–39], which is coupled to the loss of, e.g., Mn-(μ-O)$_2$-Mn motifs [39] (Section 3.2.1). Results obtained by XAS [40–46], FTIR [47-51], EPR [52–58], mass spectroscopy [57,59,60], and computational methods [61–63] eventually may provide the complementary information needed to construct a complete atomic-resolution model that includes not only the metal ion, bridging oxides and ligating residues, but also the location of water molecules, protons and oxidizing equivalents. The above and other spectroscopic techniques (see Section 2.3 and, e.g. [64–75]) also may provide insight into the reaction dynamics, i.e. the structural changes associated with advancement in the reaction cycle.

Further aspects of the crystallographic models of PSII are of relevance for photosynthetic water oxidation:

(i) The Mn complex is surrounded by a protein matrix which separates the catalyst from the thylakoid lumen, thereby

prohibiting an instantaneous equilibration (i.e., in the ps or ns time domain) of the substrates ($2H_2O$) and products ($4H^+$, O_2) with the aqueous bulk phase. There are, most likely, paths for proton release and water uptake which connect the lumenal phase to the Mn complex [25,26,76,77]. The deprotonation of the Mn complex and/or proton movements to the lumenal bulk phase seem to be relatively slow processes (>100 μs, see Sections 2.2 and 2.3) rendering the Mn complex well 'insulated' with respect to incidental proton loss or uptake. Consequently the transfer of a proton to the lumenal bulk phase may either occur before or after oxidation of the Mn complex by the Y_Z-radical, but not simultaneously.

(ii) The imidazole side chain of Y_Z is at a distance of about 7 Å to the nearest Mn ion, rendering the abstraction of an H-atom by $Y_Z^{\bullet+}$ from an Mn-ligated water molecule unlikely. (This had been proposed in the influential hydrogen-atom abstraction model of Babcock and coworkers [78,79].) Furthermore, there are no indications for a proton channel connecting Y_Z to the aqueous phase [25,26,77]. This observation in conjunction with biophysical data (see Sections 2.2 and 2.3) suggests that the $Y_Z^{\bullet}$ formation is *not* followed by release of the phenolic proton to the bulk phase and subsequent H-atom abstraction from Mn-bound water. Rather the imidazole proton may reversibly shift within a 'rocking' hydrogen bond towards His_{190} [80–85] resulting in a $[Y_Z^{\bullet}–O\cdots H–N–His_{190}]^+$ complex, which in the following is denoted as $Y_Z^{\bullet+}$.

The points (i) and (ii) are in agreement with a large body of biochemical and biophysical results. Thus we assume that (1) the inner-protein location of the Mn complex prevents direct coupling between the ET to $Y_Z^{\bullet+}$ and proton release to the aqueous phase and (2) the Y_Z-residue most likely does not abstract protons from the substrate water molecules. In the following, Y_Z is considered *not* to be an intrinsic part of the catalytic center which directly facilitates the elementary chemical steps involved in O–O bond formation. The term 'Mn complex' is used to denote an entity which comprises the $Mn_4Ca(\mu\text{-}O)_n$ core, the ligating amino-acid residues, ligated water species (H_2O, OH, O), perhaps the chloride cofactor, and all further water molecules and amino-acid residues which contribute directly to the elementary steps in dioxygen formation.

2. Basic reaction cycle

2.1. Kok's classical reaction cycle

Upon application of a sequence of saturating flashes of visible light to PSII-containing thylakoid membranes, the observed flash-number dependence of the O_2-formation yield resembles a damped period-of-four oscillation in which the yield of dioxygen formation is maximal on the third, seventh and eleventh flash [86]. In 1970, Kok and coworkers explained the flash-number dependence by their S-state model [87] (for recent review, see [88]). They concluded: "about the simplest conceivable mechanism would be a linear four quantum process in which four consecutive flashes induce four increasingly oxidized states of a trapping center ($S_{0\rightarrow4}$), each excitation adding one + charge:

$$S_0 \xrightarrow{h\nu} S_1^{+} \xrightarrow{h\nu} S_2^{2+} \xrightarrow{h\nu} S_3^{3+} \xrightarrow{h\nu} S_4^{4+} \rightarrow S_0 + O_2".$$

To explain that the yield of the third flash clearly exceeds that of the fourth flash, Kok and coworkers assumed that the S_1-state is prevalent in dark-adapted samples. The observed damping in the period-four oscillations of the O_2-yield was explained by 'misses' resulting from a less-than-unity efficiency of the photochemical reactions that causes desynchronization (or scrambling) in the S-state cycling. The Kok model mostly is depicted in form of a cycle, the so-called Kok cycle or S-state cycle (Fig. 2). Translation of the term "+ charge" into "oxidizing equivalent" is required, but otherwise most aspects of Kok's model have been confirmed. Dioxygen formation indeed requires the absorption of four light quanta and the successive accumulation of four oxidizing equivalents by a single 'trapping center', as opposed to (e.g.) the cooperation of several photosystems or catalysts. The states S_0 and S_1 are essentially dark-stable, the states S_2 and S_3 decay in the seconds and minutes regime towards the S_1-state [89,90], as proposed by Kok [87].

Two aspects of Kok's model had been mostly hypothetical in 1970 and are still under debate, namely: (i) None of the four semi-stable S-states involves partial water oxidation; (ii) a distinct S_4-state is transiently formed in which four oxidizing equivalents are accumulated by the 'catalyst' before water is oxidized. These points are addressed in Sections 2.2 and 3.2.

The experiments referred to in the following mostly involve application of saturating single-turnover flashes to PSII samples and interpretation in terms of Kok's basic model. Two experimental strategies have been used:

(i) One of the four semistable S-states is (preferentially) populated by application of a distinct number of saturating flashes, then *stabilized by freezing* in liquid nitrogen (within <1 s) and characterized in spectroscopic experiments at low temperatures.

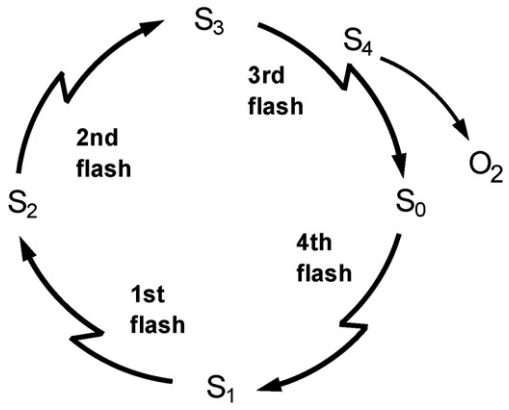

Fig. 2. S-state cycle as originally proposed by Kok and coworkers (redrawn from the inset of Fig. 6 in [87]). The S_1-state is prevalent in dark-adapted PSII. Thus the first saturating flash of light induces the $S_1 \rightarrow S_2$ transition of the catalyst in the majority of PSII.

(ii) The reactions in the four transitions between the semi-stable S-state, which proceed within the microsecond and millisecond domain, are investigated by application of *time-resolved methods at 'physiological' temperatures* (mostly 0–35 °C).

2.2. The S_4-state of the Kok cycle

The experimental methods for time-resolved X-ray absorption studies on the Mn complex of PSII have been established in a series of experiments [91–94]. On this basis, we investigated the Mn complex in its reaction cycle by time-resolved X-ray absorption measurements and detected formation of a distinct, kinetically resolvable intermediate in the $S_3 \rightarrow S_0$ transition, which is formed within about 200 μs after $Y_Z^{\bullet+}$-formation and prior to dioxygen formation [95,96] (Fig. 3). We tentatively assigned the reaction intermediate to the S_4-state of Kok [95] (see Fig. 4). The characteristics of this S_4-state, which are described in full detail elsewhere [95,96], are briefly summarized in the following (see also Fig. 3).

(1) The S_4-formation involves neither manganese oxidation nor reduction; Mn^{IV}-oxo or Mn^{V}-oxo species are not formed [95,96]. (Formation of an oxyl radical in the here discussed S_4-state, i.e. Mn-O$^{\bullet}$ instead of Mn = O, is not excluded by the time-resolved X-ray data itself, but also seems unlikely.) The absence of Mn reduction excludes that $Y_Z^{\bullet+}$ facilitates the shift towards a bound peroxide by electrostatic interactions, as it had been proposed in [80,98,99].
(2) In agreement with the time-resolved XAS data [95,96], time-resolved EPR studies [100–102] indicate that S_4-formation does not involve electron transfer from the Mn complex to the Y_Z-radical (formed in <1 μs after light absorption). Thus, at this stage three of the four oxidizing equivalents have been accumulated by the Mn complex itself whereas the fourth is located on the Y_Z radical.
(3) Central event in S_4-formation seems to be a deprotonation at the Mn complex induced by $Y_Z^{\bullet+}$. The proton is released into the aqueous phase thereby changing the charge of the Mn complex, as was proposed by Rappaport, Lavergne and coworkers on the basis of electrochromic bandshift measurements [103]. This deprotonation is an essential prerequisite for electron transfer from the Mn complex to the $Y_Z^{\bullet+}$ and thus for O–O bond formation. The proton movement to the lumen is a multi-step process where the $Y_Z^{\bullet+}$ first may induce – by long-range electrostatic interaction – the fast release of peripheral protons [104,105], then the movement of the 'defect' to the Mn complex, and eventually the crucial deprotonation at the Mn complex. The identity of the deprotonating group is unknown (see Section 3.2.7); Arg_{357} of the CP43 protein represents a plausible candidate [6,106,107].

Deprotonation of the Mn complex may be caused by both, an electrostatic 'through-space' influence of the positive charge residing on the nearby $Y_Z^{\bullet+}$ as well as by 'through-bond' effects. The distance to the Mn complex implies a sizable electrostatic effect on the pK value of the deprotonating group

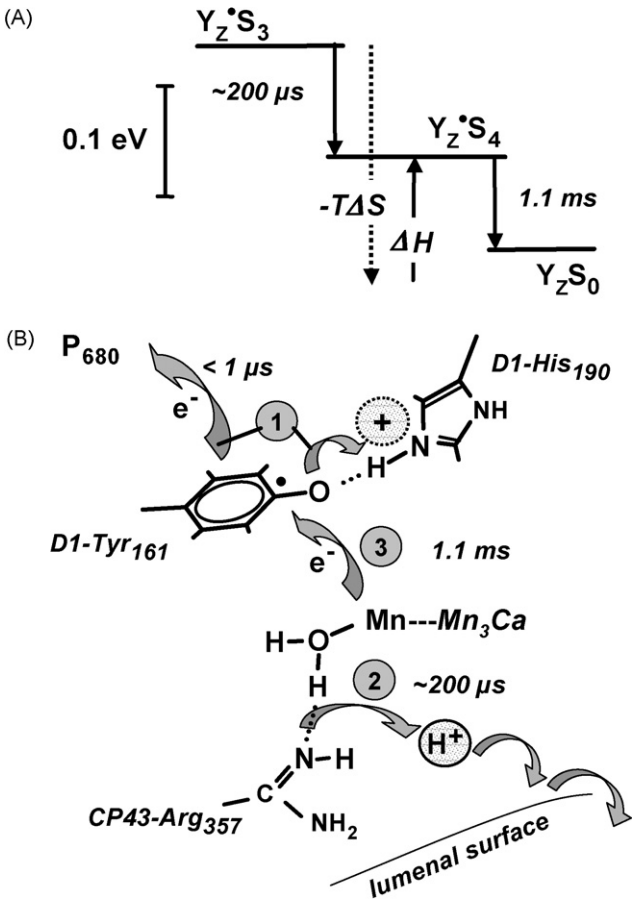

Fig. 3. S_4-formation in the $S_3 \Rightarrow S_0$ transition. (A) Energetic scheme and (B) mechanistic proposal. (A) Studies of the recombination fluorescence emitted by the chlorophyll antenna of PSII reveal that the Gibbs free energy of S_4-formation is pH-dependent and exhibits a H/D kinetic isotope effect (not shown). Its temperature dependence indicates that S_4-formation is entropically driven ($\Delta G = -0.1$ eV or -10 kJ/mol at pH 6.4 and 25 °C, $\Delta H = +0.1$ eV, $-T\Delta S = -0.2$ eV). A deprotonation close to the Mn complex and finally 'dilution' of the proton in the bulk-phase water provides the most plausible explanation of these observations. (B) Absorption of a photon is followed by Y_Z oxidation within less than 1 μs, a process coupled to a proton-shift within the hydrogen bond to the His190 of the D1 protein. The positive charge stemming from Y_Z oxidation promotes, with a halftime of about 200 μs, proton shifts and deprotonation of the CP43-Arg 357. This assignment of the deprotonating group is tentative; direct deprotonation of substrate water also is conceivable. The proton may move towards the lumenal surface along the proton path first suggested in [25]. The deprotonation at the Mn complex lowers its redox potential. Thereby the subsequent electron transfer to $Y_Z^{\bullet+}$ is facilitated, which kinetically is indistinguishable from Mn reduction and O_2 formation (identical halftimes of ~1.1 ms) (figure from [95]).

(through-space). A potentially even stronger effect could be pK-shifts mediated by covalent and hydrogen bonds (through-bond). Assuming that upon Y_Z oxidation the phenoxyl proton shifts in a hydrogen bond towards N-His_{190}, through-bond effects may be transferred by a further (bifurcated) hydrogen bond from the phenoxyl proton to a water species ligated to the calcium of the Mn complex [108]. After formation of $[Y_Z^{\bullet}\text{–O}\cdots\text{H–N–His}_{190}]^+$, also other nearby residues could play a role in mediation of a pK-shift, for example the putative Mn–ligand Glu_{189}, which is linked to His_{190} by a peptide bond.

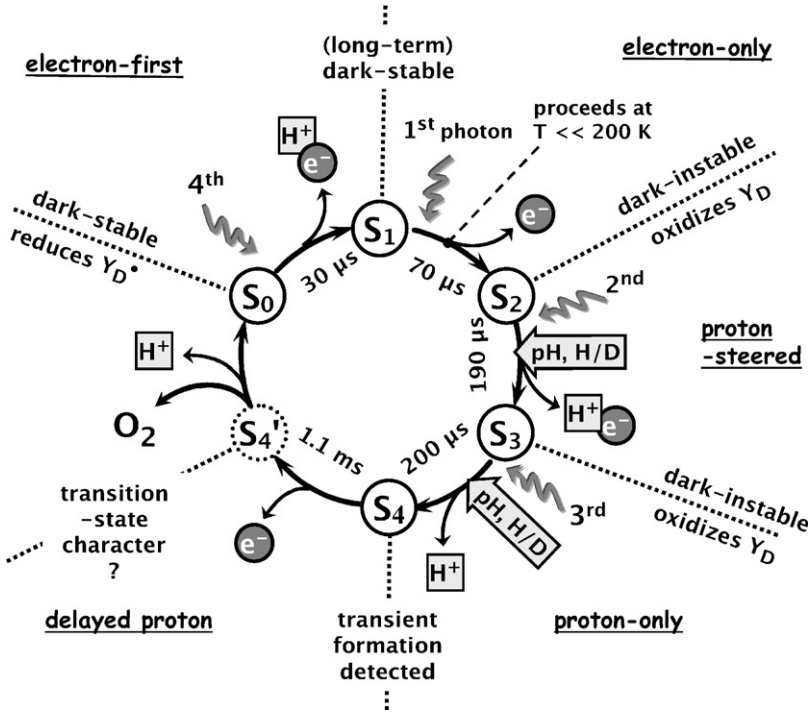

Fig. 4. Extended S-state cycle [95] and its relation to electron and proton removal in the individual S-state transitions (redrawn from [97]). A complete cycle requires sequential absorption of four photons which can be provided in form of four ns-Laser flashes. Each flash results in formation of $Y_Z^{\bullet+}$ within less than 1 μs; the subsequent processes at the PSII donor side are summarized in the shown scheme. Dark adaptation results in formation of the S_1-state in the majority of PSII so that the first flash induces the $S_1 \rightarrow S_2$ transition. For each state it is indicated whether it is dark-stable and able to oxidize or reduce $Y_D/Y_D^{\bullet}$. For each transition it is indicated whether an electron is transferred from the Mn complex to the oxidized Y_Z, whether a proton is released from the Mn complex or its ligand environment, and whether or not the rate constant is sensitive to pH and H_2O/D_2O exchange. The indicated halftimes of the S-transitions refer to the values determined in [95]. Concluding comments on the individual S-state transitions are underlined. For further details and references, see main body of the text.

In the S_4-state described above, four oxidizing equivalents have been accumulated by an oxygen-evolving complex which includes the Y_Z-residue, whereas in the preceding S-state transitions the oxidizing equivalents are accumulated by the metal complex itself (excluding Y_Z). As opposed to the preceding $S_i \rightarrow S_{i+1}$ transitions, the S_4-state is formed by a mere deprotonation event. This difference renders naming of the intermediate state as S_4 debatable as extensively discussed elsewhere ([96] and Supporting Online Text of [95]). The observation of a distinct, kinetically resolvable intermediate likely associated with proton release points to a potentially problematic aspect of Kok's reaction cycle: the exclusive focus on the accumulation of four oxidizing equivalents by electron transfer and the neglect of the equally essential role of the 'removal' of four protons (see section 2.4).

2.3. Kinetic characteristics of the S-state transitions

Each light flash causes formation of $Y_Z^{\bullet+}$, which subsequently accepts an electron from the Mn_4Ca-complex. Application of a sequence of saturating flashes of visible light, facilitates determination of the rate constants of the transitions $S_1 \rightarrow S_2$ (first flash), $S_2 \rightarrow S_3$ (second flash), $S_3 = > S_4 \rightarrow S_0$ (third flash), and $S_0 \rightarrow S_1$ (fourth flash) by time-resolved spectroscopy, namely EPR [100,101], UV/vis [99,105,109–114], and recently XAS [94,96]. Proton release has been investigated using electrodes or pH-sensitive dyes [105,115–117]. Electrochromic shifts of UV/vis absorption bands (Stark effect) of PSII pigments have provided insights into changes of the net charge of the PSII manganese complex [103,118–122]. The thus obtained experimental results are crucial for construction and evaluation of mechanistic models and summarized in the following.

2.3.1. First flash, $S_1 \rightarrow S_2$ transition

Starting in the dark-stable S_1-state, the first photon induces Mn oxidation in the $S_1 \rightarrow S_2$ transition. Initially it was found that this transition is not associated with the release of a proton [123–125]. Later non-integer and pH-dependent proton release has been explained by electrostatically triggered p*K*-shifts of peripheral bases [105,115–117,126,127]. Electrochromic studies suggest that, irrespective of pH, no charge compensating deprotonation occurs at the Mn_4Ca-complex [103,118,128,129]. The activation energy is low (~15 kJ/mol) in H_2O and D_2O [99] (12 kJ/mol in [130]) and the $S_1 \rightarrow S_2$ transition can proceed even at cryogenic temperatures [131–133]. Its rate constant is pH-independent and the kinetic isotope effect is small ($k_D/k_H \leq 1.3$) [99]. The listed properties suggest that the $S_1 \rightarrow S_2$ transition involves electron transfer from the Mn_4Ca-complex to $Y_Z^{\bullet+}$, but no deprotonation of these donor-side redox factors.

2.3.2. Second flash, $S_2 \rightarrow S_3$ transition

For the $S_2 \rightarrow S_3$ transition as initiated by absorption of the second photon, the pH-independent release of one proton as well as the electrochromism data on charge accumulation

suggest release of exactly one proton from the Mn complex [105,115–117,134]. The rate constant is pH-dependent and the kinetic isotope effect is more sizable (temperature-dependent k_D/k_H-ratio of 1.4–2.) than in the $S_1 \rightarrow S_2$ transition suggesting that the $S_2 \rightarrow S_3$ transition is 'kinetically steered' by proton movements [99]. The activation energy is clearly greater than in the $S_1 \rightarrow S_2$ transition (35 kJ/mol in H_2O and 45 kJ/mol in D_2O [99,130]) and the transition is inhibited at low temperatures [131,132]. With respect to its kinetic characteristics the $S_2 \rightarrow S_3$ transition may resemble the recently described $S_3 \rightarrow S_4$ transition which has been assigned to proton release from the Mn complex [95,96]. We have proposed [88,97] that in the $S_2 \rightarrow S_3$ transition, after formation of the Y_Z radical and before Mn oxidation, a proton is removed from the Mn complex or its immediate ligand environment; the proton release may be rate-limiting (i.e. slower than the subsequent ET step) and thus determines the experimentally accessed kinetic properties of the $S_2 \rightarrow S_3$ transition (see Section 2.4).

2.3.3. *Third flash, $S_3 \rightarrow S_4 \rightarrow S'_4 \rightarrow S_0$ transition*

Absorption of the third photon initiates the sequence of events leading to dioxygen formation and release; our current view on these events is described in the following. Prior to dioxygen formation the S_4-intermediate is formed within ~200 μs, most likely by proton release as discussed above (Fig. 3). Inhibition of this proton release step may explain the drop in the yield of the $S_3 \rightarrow S_0$ transition at low pH [135]. The subsequent electron transfer from the Mn complex to $Y_Z^{\bullet+}$ ($S_4 \rightarrow S'_4$ transition) is assumed to be the rate-limiting step in dioxygen formation ($t_{1/2}$ of about 1.2 ms); it is followed by the rapid onset of water oxidation and Mn reduction. The millisecond rate constant is pH-independent and exhibits a minor (k_D/k_H = ~1.4 [99]) or even negligible ($k_D/k_H < 1.2$ in [136]) kinetic isotope effect. In this respect it resembles the rate constant of the electron transfer in the $S_1 \rightarrow S_2$ transition, but the activation energy of the millisecond transition is clearly greater [99,130,137], which is possibly explainable by a greater reorganization energy due to more substantial structural changes of the manganese complex of PSII. Time-resolved proton release measurements suggest that a proton is released from the Mn complex in the millisecond time domain [99,105,104]. Interestingly, in D_2O [99] or at pH-values around pH 6.3 [104] the proton release seems to be delayed with respect to the Mn-reduction and dioxygen formation.

2.3.4. *Fourth flash, $S_0 \rightarrow S_1$ transition*

The fourth photon closes the described cycle by promoting the $S_0 \rightarrow S_1$ transition. Mutually not fully consistent, pH-dependent proton stoichiometries have been reported [105,115–117]. More recently Schlodder and Witt detected a pH-independent release of a single proton by microelectrode measurements on PSII core complexes of the cyanobacterium *Synechococcus elongatus* [115]. From electrochromic measurements it is clear that no charge is accumulated in the $S_0 \rightarrow S_1$ transition [118,128,129]. We conclude that the $S_0 \rightarrow S_1$ transition likely involves oxidation of the Mn complex as well as a charge-compensating deprotonation of or close to the Mn complex. As is the case for the electron transfer to the Y_Z radical in the $S_1 \rightarrow S_2$ transition, the rate constant seems to be essentially pH-independent and, in comparison to the $S_2 \rightarrow S_3$ transition, insensitive to H_2O/D_2O exchange; its activation energy is relatively low [99,130]. Thus the properties of the $S_0 \rightarrow S_1$ rate constant suggest an electron transfer which is not limited by proton movements, whereas the proton release data points towards a charge compensating deprotonation. In conclusion, the experimental results on the $S_0 \rightarrow S_1$ transition of the Mn complex can be rationalized by assuming a rate-limiting ET followed by a deprotonation step and proton release into the lumenal bulk phase.

2.3.5. *High- and low-potential S-states*

Several lines of evidence suggest that the S-states differ in their equilibrium redox potential. Whereas the S_1-state is stable in the dark and the S_0-state lifetime may reach several hours, the lifetime of the states S_2 and S_3 is in the range of tens of seconds [89,90]. Slow oxidation of the S_0-state towards the S_1-state by the Y_D-radical is possible [138], whereas in the S_2- and S_3-state the Mn complex can oxidize Y_D resulting in $Y_D^{\bullet}$ formation [139,140]. Thermoluminescence data suggests a clearly more positive potential for reduction by charge recombination of the states S_2 and S_3 (as compared to S_0 and S_1), whereas the $S_3 \rightarrow S_2$ and $S_2 \rightarrow S_1$ reduction potentials may differ by only 15 mV [73,133,140–143]. In [39] we proposed to use the rate of X-ray photoreduction as an indicator of the redox potential (or the 'electrophilicity') of the metal complex. At 20 K and at room temperature, the X-ray photoreduction rate is similar and two to three times higher in the states S_2 and S_3 as in the states S_0 and S_1 (within the uncertainty limit of the data) suggesting a more positive redox potential in the semi-stable states S_2 and S_3, on the one hand, than in the states S_0 and S_1, on the other hand (Table 1). Also further experimental observations may be related to the presence of two high-potential (S_2 and S_3) and two low-potential (S_0 and S_1) states of the Mn complex, e.g. the susceptibility of the Mn complex to UV irradiation [144]).

In conclusion, comparing the four semi-stable S-states of the Mn complex we find that the states S_0 and S_1, on the one hand, and the states S_2 and S_3, on the other hand, differ with respect to several properties which are presumably related to the equilibrium redox potential of the Mn complex. The listed evidence points towards a more positive potential in the states S_2 and S_3 than in the states S_0 and S_1.

Some aspects of the heterogeneity in the properties of the individual S-state transition are schematically summarized in Fig. 4.

2.4. *Cycle of alternate H^+/e^- removal from the Mn complex*

In 1970, Kok and coworkers have described the accumulation of four oxidizing equivalents at the donor side of PSII by means of their seminal S-state model [87] (Section 2.1). Only the S_4-state formation, i.e. the accumulation of a fourth oxidizing equivalent prior to the onset of water oxidation, defied experimental verification. In 1970, Kok could not specify the entity which accumulates the oxidizing equivalents because neither the role of the Mn complex nor of the Y_Z-residue had been

Table 1
S-state dependence of X-ray photoreduction at 20 K and room temperature (RT)

n_{flash}	Predominant S-state before irradiation	X-ray reduction rate at 20 K (r.u.)	X-ray reduction rate at RT (r.u.)	Structural change upon one-electron reduction at 20 K
0	S_1	1.0	1.0	$S_1 \rightarrow S_0$*: loss of Mn–(μ-O)$_2$–Mn motif
1	S_2	2.2	2.8	$S_2 \rightarrow S_1$*: no bridging-mode change
2	S_3	2.0	3.3	$S_3 \rightarrow S_2$*: loss of Mn–(μ-O)$_2$–Mn motif(s)
3	S_0 (∼50%)	1.4	1.8	$S_0 \rightarrow S_{-1}$*: unknown

The given photoreduction rates have been reported in the Supporting Online Material of [145]; the given values are not corrected for misses so that after three flashes only about 50% of the PSII is in the S_0-state. The photoreduction rates are normalized to the S_1-state rate, the estimated uncertainty in these numbers is on the order of ±25%. The suggested structural changes are described in [39] or represent unpublished results.

established. Today the accumulator is considered to be either (i) an entity consisting of the Mn complex plus Y_Z or (ii) the Mn complex alone. These two options render unclear whether the S_4-intermediate described in Section 2.2 is (in the case of option i) or is not (option ii) the S_4 state of Kok. In an attempt to deal with this ambiguity, we have involved an S_4 and an S'_4 state [95] (Fig. 4). In both of these the Mn complex/Y_Z entity has accumulated four oxidizing equivalents (and both differ from the S_3-state likely by a chemical change involving proton release), but in the S_4 state the fourth oxidizing equivalent is located on the Y_Z-residue ($Y_Z^{\bullet+}$) whereas in the S'_4 state it has moved to the Mn complex itself. This extension of Kok's classical cycle may appropriately describe the results we have reported elsewhere [95,96], but overall is insufficient for explaining a larger body of experimental observations.

The mechanistic discussion of the energetics and kinetics of photosynthetic water oxidation may profit by an extension of Kok's cycle towards a basic model which addresses not only the accumulation of four oxidizing equivalents explicitly, but also the removal of four protons from the Mn complex [88,97]. The extended reaction cycle shown in Fig. 5 is not exceedingly complex. This is because the results reviewed above (Section 2.3) point towards a simple principle which underlies the reaction cycle shown in Fig. 5: protons and electrons are removed strictly alternately from the Mn complex. Here 'removal' of a proton means deprotonation of the Mn complex – including the Mn–ligand environment but *excluding* Y_Z – and transfer of this proton to the lumenal bulk phase whereas electron-removal denotes oxidation of the Mn complex by electron transfer to the previously formed Y_Z radical. The four proton-release steps and the four oxidation steps result in a total of eight steps that precede dioxygen formation [88,97].

Previously we have denoted the involved nine intermediate states of the Mn complex in the scheme of Fig. 5 as I-states, where I_0 denotes the Mn complex immediately after dioxygen release and I_8 the Mn complex after removal of four electrons and four protons and immediately before the O–O bond formation [88,96,97]. However, we found that – after decades of S-state studies – the I-state nomenclature is mnemonically problematic and may not be easily acceptable to researchers in the field. Therefore, here a nomenclature is used where the nine I-states are replaced by nine S-states (Fig. 5), namely: S_0^+ (I_0), S_0^n (I_1), S_1^+ (I_2), S_1^n (I_3), S_2^+ (I_4), S_2^n (I_5), S_3^+ (I_6), S_3^n (I_7), and S_4^+ (I_8). In this modified S-state terminology, the subscript indicates the number of oxidizing equivalents accumulated by the Mn complex (excluding Y_Z) and the superscript indicates the relative charge which is either positive (+) or neutral (*n*). The charge decreases in each proton release step and increases by Mn-complex oxidation by ET to $Y_Z^{\bullet+}$. In the extended S-state cycle of Fig. 5, the Mn complex is assumed to be neutral in the classical states S_0 and S_1 (now S_0^n and S_1^n), but positively charged in the classical S_2 and S_3 (now S_2^+ and S_3^+). For a

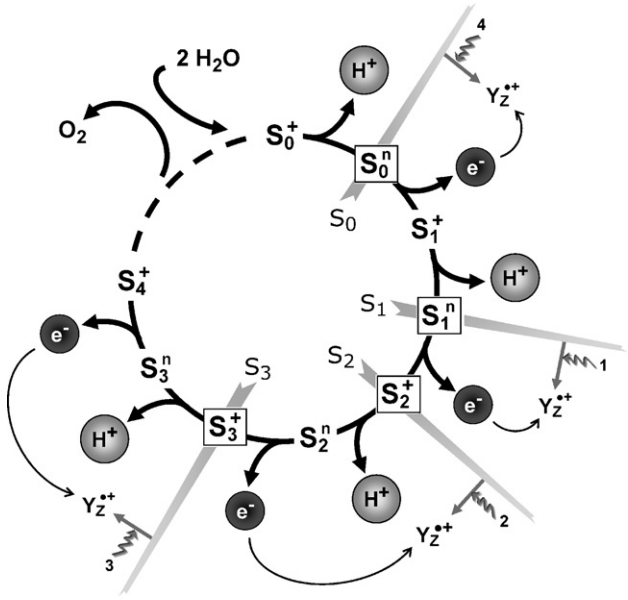

Fig. 5. Cycle of alternating removal of protons and electrons from the Mn complex [97]. Electrons and protons are removed from a Mn complex which comprises the $Mn_4Ca(\mu\text{-}O)_n$ core, the protein environment and bound water molecules; Y_Z is considered to be not an intrinsic part of the Mn complex. The nine intermediate states of the Mn complex are denoted as $S_i^{+/n}$-states where the subscript gives the number of accumulated oxidizing equivalents and the superscript indicates the relative charge (positive (+) or neutral (n) relative to the dark-stable S_1-state). Four S-states are stable for tens of seconds: S_1^n (fully dark-stable), S_2^+, S_3^+, and S_0^n. The special semi-stable character of these S-states is emphasized by an enclosing rectangle; they correspond to the classical S-states, namely S_1, S_2, S_3, and S_0. Starting in any of these four semi-stable S-states, a saturating flash of visible light induces formation of $Y_Z^{\bullet+}$. For light-flash application in the S_2^+ and S_3^+ state, $Y_Z^{\bullet+}$ formation results in release of a proton from the Mn complex into the aqueous phase; only subsequently an electron is transferred from the Mn complex to $Y_Z^{\bullet+}$. The shown reaction cycle has been presented previously [88,96,97] using a nomenclature where the nine states from S_0^+ to S_4^+ were numbered consecutively and denoted as $I_0, I_1, \ldots, I_8$. The proposed regular sequence of alternating deprotonation and oxidation steps straightforwardly explains the irregular properties of the individual transitions of the S-state cycle shown in Fig. 4.

schematic representation of the relation between redox-potential and $S_i^{+/n}$-state, see [88].

The regular sequence of electron and proton removal steps qualitatively can explain the intricate properties of the individual S-state transitions (compare Figs. 4 and 5), as briefly outlined in the following (see also [88]) and detailed with respect to the realization at the atomic level in Section 3.

(I) In the $S_0 \rightarrow S_1$ transition, oxidation of the Mn complex by $Y_Z^{\bullet}$ ($S_0^{n} \rightarrow S_1^{+}$, $E_m \sim 1$ V) causes a shift in the pK value of an intrinsic base, e.g. a μ-OH group [40,145,146], and thus is followed by the release of a proton ($S_1^{+} \rightarrow S_1^{n} + H^{+}$). By this deprotonation the redox potential of the Mn complex is lowered so that the next oxidation again can proceed at ~1 V.

(II) The $S_1 \rightarrow S_2$ transition exclusively involves oxidation of the Mn complex ($S_1^{n} \rightarrow S_2^{+}$) so that (i) a positive charge is acquired by the complex (S_2^{+}) and (ii) the E_m for the next oxidation by $Y_Z^{\bullet+}$ would be too high (>1.1 V).

(III) Subsequent $Y_Z^{\bullet+}$ formation causes a shift of pK values at the nearby Mn complex such that one proton is released ($S_2^{+} \rightarrow S_2^{n} + H^{+}$). Thereby the E_m value is lowered significantly so that the ET step can proceed ($S_2^{n} \rightarrow S_3^{+}$).

(IV) Subsequent $Y_Z^{\bullet+}$ formation causes a shift of pK values at the nearby Mn complex such that one proton is released ($S_3^{+} \rightarrow S_3^{n} + H^{+}$). Thereby the E_m value is lowered significantly so that the ET step can proceed ($S_3^{n} \rightarrow S_4^{+}$). This ET step is kinetically not separable from Mn reduction and dioxygen formation in the $S_4^{+} \rightarrow S_0^{+}$ transition. Coupled dioxygen formation and Mn reduction ($S_4^{+} \rightarrow S_0^{+}$), binding of a new set of substrate-water molecules, and reorganisation of the Mn complex are followed by the release of a fourth proton ($S_0^{+} \rightarrow S_0^{n} + H^{+}$) thereby reverting the charge accumulation of the $S_1 \rightarrow S_2$ transition.

By assuming alternating removal of protons and electrons from the Mn complex the properties of the classical S-state transitions are straightforwardly rationalized, as the reader may confirm by a step-by-step comparison of Figs. 5 and 4.

The simplicity of the underlying principle (of strictly alternate proton and electron removal) should not obscure that the events following $Y_Z^{\bullet+}$ formation depend on the state of the Mn complex in a rather intricate way. For a detailed discussion of the remarkable dual role of $Y_Z^{\bullet+}$, see [88]. Briefly, in the $S_0 \rightarrow S_1$ and $S_1 \rightarrow S_2$ transition, $Y_Z^{\bullet+}$ formation is followed by electron transfer ($Y_Z^{\bullet+}$ as an electron acceptor). In the transitions $S_2 \rightarrow S_3$ and $S_3 \rightarrow S_4 \rightarrow S_0$, $Y_Z^{\bullet+}$ formation causes proton release from the Mn complex—mediated by electrostatic through-space or through-bond influences on pK values ($Y_Z^{\bullet+}$ as an electrostatic promoter). This proton release precedes the ET to $Y_Z^{\bullet+}$ as suggested by the experimental results on the transition $S_3 \rightarrow S_4$ transition (see Section 2.2) and predicted by the reaction cycle of Fig. 5 for the $S_2 \rightarrow S_3$ transition. The switch to a *proton-first ET* results from the lack of a deprotonation in the $S_1 \rightarrow S_2$ transition. Why specifically the $S_1 \rightarrow S_2$ transition lacks an associated deprotonation, remains an open question.

In the extended S-state cycle four deprotonation and four electron transfer reactions precede dioxygen formation, which can be described by the following equations:

$$S_0^{+} \leftrightarrow S_0^{n} + H^{+}\,(\text{bulk}) \quad (1)$$

$$S_0^{n} + Y_Z^{\bullet+} \leftrightarrow S_1^{+} + Y_Z \quad (2)$$

$$S_1^{+} \leftrightarrow S_1^{n} + H^{+}\,(\text{bulk}) \quad (3)$$

$$S_1^{n} + Y_Z^{\bullet+} \leftrightarrow S_2^{+} + Y_Z \quad (4)$$

$$S_2^{+}[+Y_Z^{\bullet+}] \leftrightarrow S_2^{n}[+Y_Z^{\bullet+}] + H^{+}\,(\text{bulk}) \quad (5)$$

$$S_2^{n} + Y_Z^{\bullet+} \leftrightarrow S_3^{+} + Y_Z \quad (6)$$

$$S_3^{+}[+Y_Z^{\bullet+}] \leftrightarrow S_3^{n}[+Y_Z^{\bullet+}] + H^{+}\,(\text{bulk}) \quad (7)$$

$$S_3^{n} + Y_Z^{\bullet+} \leftrightarrow S_4^{+} + Y_Z \quad (8)$$

$$S_4^{+} + 2H_2O|_{\text{next}} \leftrightarrow S_0^{+} + O_2\nearrow \quad (9)$$

The symbol $S_i^{+/n}$ refers to the Mn complex and its relevant ligand environment, including the two bound substrate-water molecules.

In Eq. (9), we refer to the binding of the substrate water for the next turnover of the reaction cycle. Thus the O_2 molecule indicated on the right side of Eq. (9) is not formed by oxidation of the water indicated on the left side of Eq. (9). Because it is not known definitively where in the reaction sequence the two substrate water molecules bind, the inclusion of water binding in Eq. (9) is speculative. Inclusion in Eq. (9) implies that the corresponding binding energy can promote the dioxygen-formation and detachment step, a hypothetical but plausible conjecture. We also note that the reaction described by Eq. (9) may involve several 'internal' reaction intermediates, i.e. transiently formed conformations of the Mn complex, including the substrate-water atoms, e.g. the peroxidic state suggested by experiments at elevated O_2 pressure [147,148].

The Eqs. (1)–(8) refer to alternating ET and proton release steps. The energetics of each step is describable either by a pK value of the deprotonating group of the Mn complex (Eqs. (1), (3), (5) and (7)) or a difference in Gibbs free energy (ΔG) which can be related to the redox-potential difference between the respective $Y_Z/Y_Z^{\bullet+}$ and S_i^{n}/S_{i+1}^{+} couples (Eqs. (2), (4), (6) and (8)). Due to the spatial separation of the Mn complex from the lumenal bulk phase, the ET steps are kinetically separated from the proton release. However, it is not excluded that in the four redox reactions, electron transfer is directly coupled to proton movements *within* the Mn-complex entity. Specifically the ET in the $S_2 \rightarrow S_3$ transition (Eq. (6)) may involve such a concerted electron-proton transfer. The rate constant of this transition exhibits a kinetic isotope effect which is greater than in any other S-state transition, but presumably too small ($k_{H_2O}/k_{D_2O} < 2$) for a rate-limiting contribution of nuclear tunneling by the proton [149–152]. Proton movement within a strong hydrogen bond which is kinetically limited by the reorganisation of heavier atoms might explain the relatively weak H/D isotope effect. Further studies are required to clarify this important point. Irrespective of how the ET is coupled to internal reorganisation of the Mn complex, redox potentials (or at

least ΔG-values) can be assigned to the ET reactions of Eqs. (2), (4), (6), and (8).

With the possible exception of the S_4^+-state, which could resemble a transition state, all intermediates of the reaction cycle are proposed to be real intermediates which are either semi-stable (S_0^n, S_1^n, S_2^+, S_3^+) or formed transiently (S_0^+, S_1^+, S_2^n, S_3^n). These eight states of the Mn complex may represent a useful framework for theoretical studies on the four ET reactions and the four proton-release steps. Experimental results on the transient formation of the S_3^n-state (i.e. the S_4-state in [95]) have been reported [95,96,103,153,154]. Experimental characterization of the transiently formed states S_2^n, S_0^+, and S_1^+ likely is particularly challenging, but is required in order to leave the realm of the hypothetical.

2.5. Energetic constraints of PSII water oxidation

The equilibrium electrode potential, E_m, of the reaction:

$$2H_2O(aq) \leftrightarrow O_2(g) + 4H^+(aq) + 4e^- \quad (1.229\,V) \qquad (10)$$

at pH 0 is ~1.23 V (against NHE), at room temperature and in the presence of 100 kPa gaseous dioxygen. At atmospheric O_2 partial pressure of 21 kPa the value is lower by 1/4 of 0.04 V resulting in an E_m^0 of 1.22 V. At this potential the rates of water oxidation and dioxygen reduction are equal; for net water oxidation, an overpotential is required ($E > E_m$).

The value of E_m depends on pH according to (at ~300 K):

$$E_m \approx 1.22\,V - 0.06\,V\,pH \qquad (11)$$

because the reverse reaction, i.e. dioxygen reduction, is favored by higher proton concentrations. Alternatively the decrease in E_m at higher pH can be understood as an entropic contribution to the equilibrium potential which relates to the 'dilution' of protons in the aqueous medium. In PSII, the maximal (lumenal) proton concentration for residual dioxygen formation may correspond to a pH of 4.2 [155] and thus to an equilibrium potential of ~0.97 V. (For results on the inhibition of the individual S-state transitions at low pH, see Ref. [135].)

The potential of the primary oxidant, $P680^+$, recently has been estimated to be close to 1.25 V [65,156] and thus is more positive than previously thought (for a discussion, see [156]). The uncertainty range in this value is unclear, but presumably below ±0.05 V [65]; in the following estimates, the uncertainty range of this and other literature values is not considered. The potential of $Y_Z^{\bullet+}$ is S-state dependent and changes with time [84,157–159], presumably explainable by changes in the E_m of $Y_Z^{\bullet+}$ which relate to inner-protein proton movements and release. After the third flash, e.g., the $Y_Z^{\bullet+}$ potential at ~10 μs may be 1.21 V [65,158] and it drops further by ~0.09 V in the $S_3^+ \rightarrow S_3^n$ transition [95,154] to a value of ~1.12 V. In the $S_1 \rightarrow S_2$ and $S_0 \rightarrow S_1$ transitions, on the one hand the Y_Z-potential at 10 μs is less positive than 1.21 V [65,157–159], on the other hand the subsequent potential-drop due to proton movements is clearly smaller than 0.09 V. Thus we estimate that in all S-state transitions the $Y_Z^{\bullet+}/Y_Z^0$ potential for oxidation of the Mn complex is not significantly higher than 1.1 V. Assuming a free-energy loss associated with oxidation of the Mn complex of at least 0.05 V [160], we arrive at an estimate of ~1.05 V for the potential of the Mn complex when it is oxidized by $Y_Z^{\bullet+}$. Comparison of the E_m of the electrode reaction (4×0.97 V at pH 4.2) and the oxidizing power supplied by oxidation of the Mn complex (4×1.05 V) indicates that photosynthetic water oxidation by the Mn complex is energetically highly efficient.

The above equilibrium considerations tend to obscure an aspect discussed by Krishtalik already in the eighties, namely the role of proton release in the energetics of PSII water oxidation [161–164]. Krishtalik considered the following situation: In the elementary step of water oxidation, four oxidants facilitate the four-electron oxidation of water which is coupled to the transfer of 4 protons (from the two substrate water) to 4 water molecules (formation of four H_3O^+ ions). Furthermore dioxygen is formed at the active site. Since the proton and dioxygen release are necessarily delayed with respect to the elementary steps of water oxidation, the starting point for the reversal of the elementary reaction are four H_3O^+ and one O_2 molecule which are in the active site and close to the catalyst. Thus, the midpoint potential for the elementary step is not given by Eq. (11), but requires a correction for the drastically increased proton and dioxygen concentrations. Thereby the configurational potential, E_c, of Krishtalik is obtained:

$$\begin{aligned} E_c &= E_m^0 + \Delta E\,(O_2\ \nearrow) + \Delta E\,(H^+\ \nearrow) \\ E_c &= 1.23\,V + 0.07\,V + 0.10\,V = 1.40\,V. \end{aligned} \qquad (12)$$

This means that the potential of the four oxidants in the elementary step would need to exceed 1.4 V. Recent experiments on O_2 formation at elevated pressure lead to the suggestion that the entropy gain due to dioxygen release (0.07 V) might contribute to the driving force of the elementary reactions [147,148] so that the relevant configurational potential possibly rather is 1.33 V than 1.4 V. In any event, E_c is clearly greater than the oxidation potential of the Mn complex ($E_m \sim 1.05$ V in the ET to $Y_Z^{\bullet+}$).

On a first glance, Krishtalik's considerations seem to point to a paradox. On the one hand the entropy gain due to proton dilution is required to match the tight energetic constraints of photosynthetic water oxidation, on the other hand it cannot promote the elementary reaction of dioxygen formation itself. This paradox can be resolved only by taking into account proton release from the catalytic center (i.e. the Mn complex including bound substrate-water molecules) already in the steps of the reaction cycle which precede dioxygen formation [161–164]. In these either a substrate-water molecule or another group of the catalytic center is deprotonated. In the first case, protons from the substrate water are already released prior to dioxygen formation. In the latter case, the bases formed by proton release could serve as proton acceptors in the dioxygen-formation step thereby contributing to the driving force of this elementary reaction. In both cases, the binding energy of the proton released from the Mn complex represents a favorable contribution to the energetic demands of the elementary dioxygen-formation step.

Its magnitude can be estimated according to (at ~300 K):

$$\Delta E_{\mathrm{bind}}^{\mathrm{H+}} = (\mathrm{p}K_{\mathrm{base}} - \mathrm{p}K_{\mathrm{H_2O}})\ln(10)\frac{RT}{F} \approx (\mathrm{p}K_{\mathrm{base}} + 1.74)\,0.06\,\mathrm{eV} \quad (13)$$

where $\Delta E_{\mathrm{bind}}^{\mathrm{H+}}$ is the binding energy of the proton to the base created in reactions (1), (3), (5), or (7) minus the binding energy of a proton to a single bulk-water molecule.

Assessment of the energetic constraints of water oxidation is facilitated by the nine-step reaction sequence discussed above. The oxidation of the Mn complex described by Eqs. (2), (4), (6), and (8) likely proceeds at a potential of ~1.05 V. Because water oxidation may proceed down to pH-values of ~4.2, albeit at minimal rates, the maximal pK of the deprotonation reactions described by Eqs. (1), (3), (5), and (7) may be close to 4.5. According to Eq. (13), this corresponds to a gain in potential for the elementary reaction of dioxygen formation of ~0.37 V per base. Thus, by reactions (1)–(8) a driving force for the dioxygen-formation step of about 4 × 1.42 V is created. Taking into account that, as opposed to Krishtalik's original analysis, dioxygen release may contribute to the energetics of the elementary steps (thus, E_c = 1.33 V), the value of 1.42 V is sufficiently high to render water oxidation energetically feasible, however only by a narrow margin. The small driving-force surplus requires that exactly four protons are set free from the Mn complex before onset of the elementary reaction step(s) of O=O bond formation. We note that proton release from a base close to the Mn complex, but too distant to contribute directly to the elementary reactions, would be insufficient.

The above considerations are not flawed by the potential-lowering effect of the deprotonation [165] or the complex relation between protonation state and redox potential in general. This becomes obvious by considering the free-energy losses after light-induced formation of $Y_Z^{\bullet+}$ which are approximately given by (for one pair of electron/proton removal steps; e, elementary charge):

$$|\Delta G_{\mathrm{loss}}| \approx e(E_{\mathrm{m}}(Y_Z^{\bullet+}/Y_Z) - E_{\mathrm{m}}(S_{i+1}{}^{+}/S_i{}^{n})) + (\mathrm{pH} - \mathrm{p}K_{\mathrm{base}})0.06\,\mathrm{eV}, \quad (14)$$

where pK_{base} refers either to bound substrate water or to a base that later accepts a substrate proton in the O_2-formation step. Consideration of the respective free-energy losses results in conclusions on the energetic constraints of water oxidation which are identical to the ones described in the preceding two paragraphs, as the reader may verify by application of Eq. (14).

We conclude that energetic considerations on photosynthetic water oxidation need to account explicitly for the essential contribution of proton-release steps. Extension of Kok's cycle to a nine-step reaction cycle (Fig. 5, Eqs. (1)–(9)) facilitates incorporation of the proton-release contributions into energetic considerations in a reasonably simple, straightforward way.

In summary, the given energetic constraints of water oxidation by the Mn complex of PSII suggest: (i) for each of the four oxidations, the E_m of the Mn complex is close to 1.05 V in the actual ET step. (ii) Not only four oxidation steps, but also four interlaced deprotonation steps precede dioxygen formation. These are likely characterized by pK-values around 4.5.

The deprotonation reactions may not only be an energetic requirement with respect to the dioxygen formation step itself, but also be pivotal in facilitating four successive oxidations of the Mn complex at about the same potential, as outlined in the following.

3. Realization at the atomic level

3.1. Constancy of redox potential

The mostly oxidation-state independent redox potential of the Mn complex in the ET to the Y_Z radical is remarkable. If the four Mn ions were electronically isolated, we might observe (e.g.) four essentially independent $Mn^{III} \rightarrow Mn^{IV}$ oxidations at the same redox potential. However, not only that four isolated Mn ions are an unlikely water oxidant, the short Mn–Mn distances found by EXAFS [37,46,145,166–171] as well as the analysis of EPR results [52,172–177] are highly suggestive that the four Mn ions are strongly coupled, most likely via bridging oxygen atoms. Consequently, any oxidation of one Mn ion is predicted to increase the oxidation potential for the next single-electron oxidation of the complex significantly as summarized for sets of mono-μ-oxo and di-μ-oxo bridged Mn_2-complexes in [178,179] (increase in E_m by 0.5 to >1.0 V), and exemplified also by the first oxidation step in Fig. 6 [180]. In PSII, a comparable potential increase would prevent subsequent oxidation steps of the Mn complex.

Fig. 6 does not only illustrate the 'redox-potential problem' [165], but also a possible solution: the formation of an additional μ-oxo bridge between Mn ions effectively prevents the potential increase (for details see [180]). We note that the formation of new μ-oxo bridges in response to Mn oxidation (see, e.g. [181–185]) likely involves (de)protonation events, but quantitative information on this point is rare (e.g. relevant pK-values). Also the potential-lowering effect of μ-oxo bridge formation by deprotonation of already existing μ-hydroxo bridges is well established [183,186–191]. In the binuclear Mn complex studied by [192], the potential increase upon Mn oxidation is limited to only 0.15 V by the deprotonation of a terminally coordinated water molecule. However, in PSII even such a minor potential increase would prohibit oxidation of the Mn complex by $Y_Z^{\bullet+}$.

The transformation of a μ-OH bridge to a μ-O bridge may counteract a potential increase as illustrated in Fig. 7 (typical values for pK-changes upon oxidation from [191]). The first Mn-oxidation on A → B results in a redox-potential increase by 0.5–1.2 V for B → E, the second purely oxidizing transition. Deprotonation of the μ-OH bridge (B → C), however, leads to a decrease in the potential for the second oxidation step (C → D) by more than 0.5 V. Thus, if the first oxidation step is coupled to (or followed by) a μ-OH deprotonation (amounting to a transition from A to C), the second oxidizing transition (C → D) will proceed at about the same potential as the first one.

Further model-chemistry studies are required to obtain quantitative information how the almost complete constancy

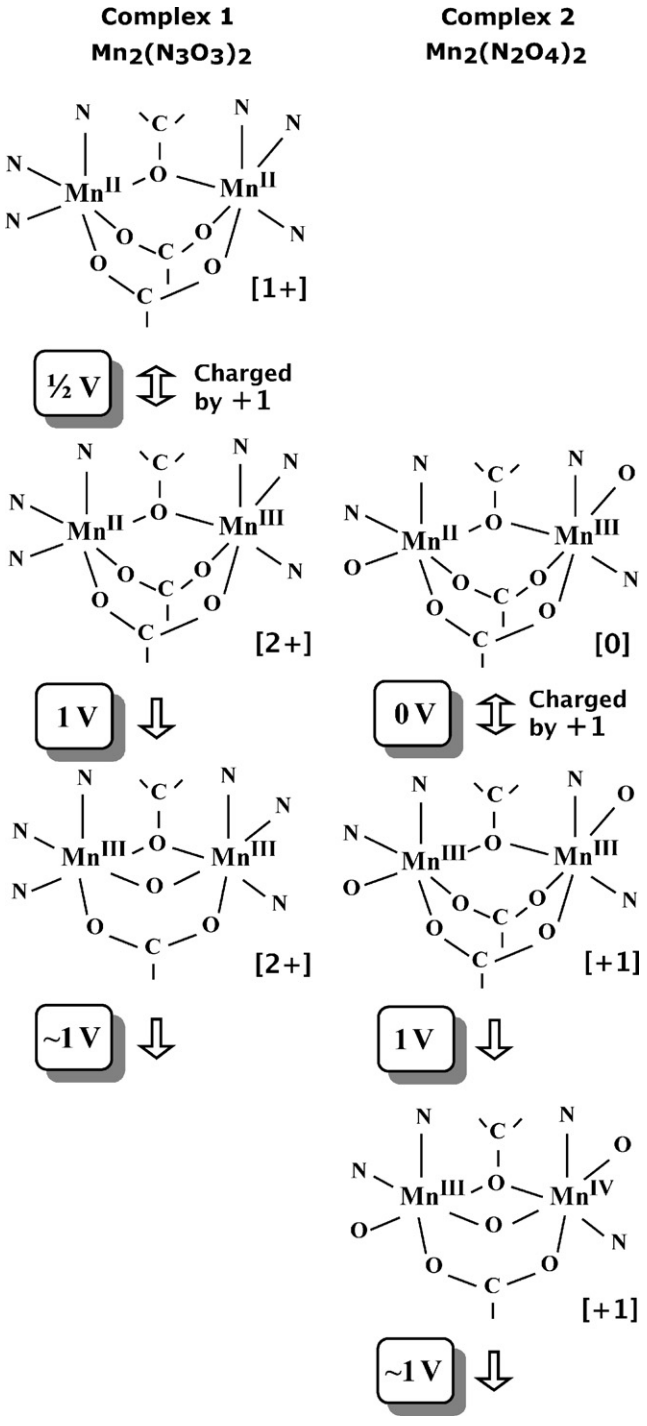

Fig. 6. Schematic representation of the structural and oxidation state changes upon sequential electrochemical or photochemical oxidation of two dinuclear Mn complexes with different N/O ratios in the primary ligand spheres of the Mn ions (modified from [180]). The approximate redox potentials of the respective transitions are indicated.

of the redox potential, as it seemingly is realized in PSII, can be achieved. It would be of special interest (e.g.) to determine whether deprotonation of a terminally coordinated water could be sufficient to ensure essentially complete compensation of the potential increase resulting from Mn oxidation.

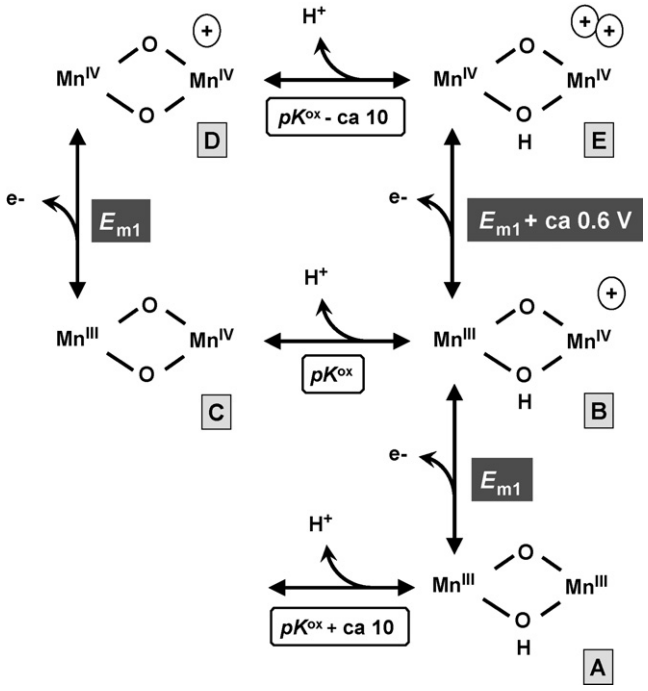

Fig. 7. Illustration of the relation between pK of μ-O bridge and midpoint potentials for a di-μ-oxo bridged Mn_2-unit. The vertical transitions refer to oxidation/reduction; the horizontal transitions to deprotonation/protonation. The B–C–D–E transitions constitute a thermodynamic cycle meaning that the difference in the pK-values corresponds to the difference in the involved midpoint potentials ($\Delta E_m \approx 60$ mV ΔpK) (modified from [165]).

In summary, any pure oxidation of the Mn_4Ca complex of PSII which proceeds without associated chemical change is predicted to cause an increase in the potential to a level that is prohibitively positive. The formation of unprotonated μ-oxo bridges either by deprotonation of a μ-OH bridge or by the formation of an additional μ-O bridge represent chemical changes that may counteract efficiently the potential increase.

3.2. Structure and oxidation states of the Mn complex in its S-state cycle

3.2.1. Modifications by X-ray exposure

Crucial information on the structure of the Mn complex of PSII comes from two techniques which nowadays both rely on the use of intense synchrotron radiation, namely X-ray absorption spectroscopy (XAS) [43,44,193,194] and protein crystallography by X-ray diffraction (XRD). The use of high doses of ionizing radiation renders radiation-induced modifications of the Mn complex – also discussed as X-ray photoreduction (of the high-valent Mn ions) or simply radiation damage – an important concern. Specifically the significance of (all) the crystallographic results on the structure of the Mn complex [23–27] can only be judged by taking into account the influence of radiation-induced modifications, which have been investigated by X-ray absorption spectroscopy (XAS) at the Mn K-edge [37–39].

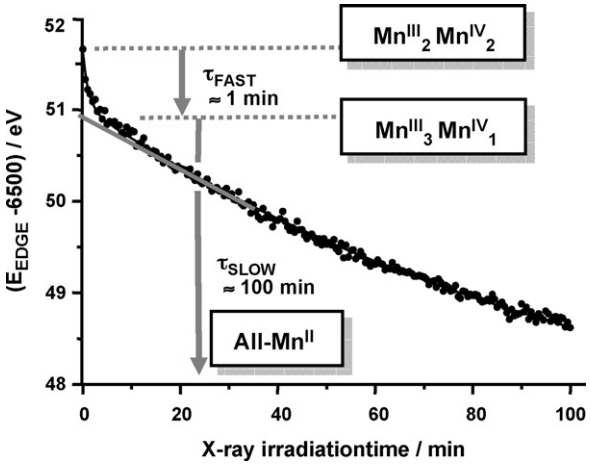

Fig. 8. Photoreduction at 10 K of the Mn-complex in its S_1-state (measured at a high-flux beamline). Decrease of the Mn K-edge energy derived from 90 successive XAS scans of 30 s duration each. A biphasic simulation yielded time constants of ∼1 and ∼100 min for the fast and slow decay phase, respectively. Note that the amplitude of the initial, fast decay of the K-edge energy corresponds to a one-electron reduction of the Mn complex. The slow phase of X-ray photoreduction eventually leads to a state where all four Mn ions have been reduced to the Mn(II) level (modified from [39]).

The X-ray absorption spectrum comprises the XANES (X-ray absorption near-edge structure, the edge-region of the spectrum) and EXAFS (extended X-ray absorption fine-structure) regions [194,195]. The information content of the XANES and EXAFS with focus on the PSII manganese complex is reviewed in [42]; see [37] for a discussion of pitfalls in the EXAFS analysis and [145] for a comprehensive presentation of data on all four semi-stable S-states. For further reviews of XAS results on the Mn complex of PSII manganese, see [40,41,44,45,196–199].

Even at cryogenic temperatures (e.g. 20 K) and relatively low flux (∼10^9 photons mm^{-2} s^{-1}), X-ray photoreduction of the Mn complex has been observed [168,200]. In crystallographic diffraction experiments on PSII, often 10^3–10^5 times higher doses are used. In [37], we have concluded that the structural information obtained by protein crystallography refers to a situation where the Mn ions are almost completely reduced to the Mn^{II}-level, a process which is coupled to the loss of di-μ-oxo bridges. In [38], X-ray photoreduction was investigated at various temperatures by XAS on PSII crystals. The S-state dependence of the photoreduction rate at 20 K and room temperature has been reported in [145] (see also Table 1). Recently flux- and temperature dependence have been studied in detail and discussed with respect to the underlying physical mechanisms [39].

At low temperatures the Mn photoreduction is pronouncedly biphasic (Fig. 8). The rapid phase accounts for reduction by one equivalent; the subsequent photoreduction is, at 20 K, by a factor of hundred slower [39]. (We note that in [38] the fast one-electron reduction has not been resolved.) EXAFS analysis suggests that, for PSII initially in its S_1-state, the rapid photoreduction phase is associated with the loss of a di-μ-oxo motif presumably coupled to the appearance of a longer Mn–Mn distance (asterisks in Fig. 9) [39].

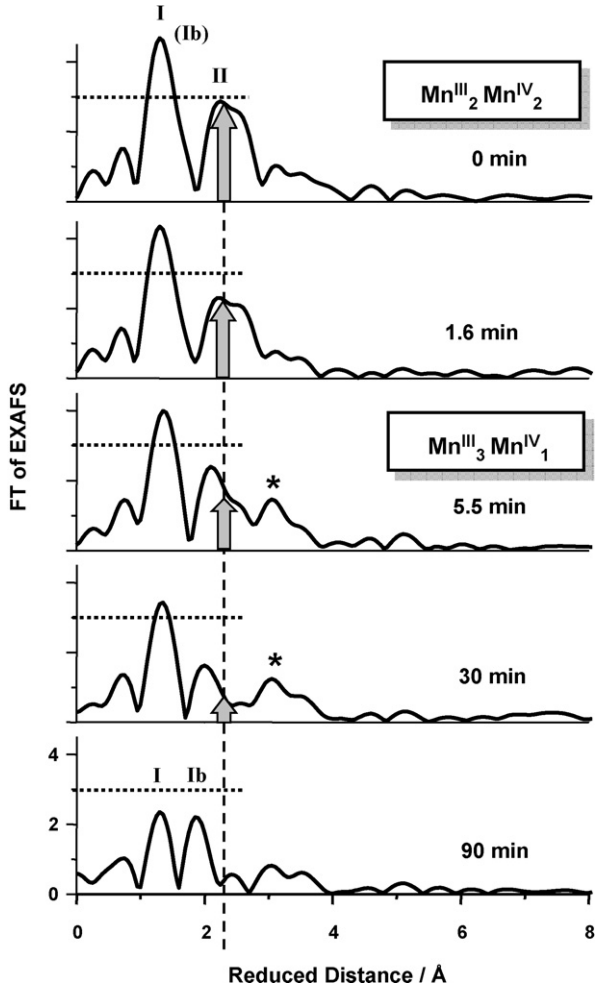

Fig. 9. Fourier-transformed EXAFS spectra collected after various X-ray exposure times (at $T < 20$ K). The top spectrum (0 min) corresponds to the Mn-complex in its S_1-state. In all other spectra, the PSII sample had been exposed to X-ray irradiation for the indicated period (modified from [39]).

The rapid X-ray photoreduction by about one reducing equivalent is observed in all S-states, however the rate and the associated structural changes are S-state dependent (Table 1). As opposed to the $S_1 \rightarrow S_0$* transition, the $S_2 \rightarrow S_1$* transition is not associated with the loss of a di-μ-oxo bridge (unpublished results), in accord with the suggested absence of structural changes upon oxidation of the Mn complex in the light-induced $S_1 \rightarrow S_2$ transition. Starting in the S_3-state, the one-electron reduction is as fast as in the S_2-state, but is coupled to particularly pronounced structural changes which may even amount to the loss of more than one di-μ-oxo motif (unpublished results). Consequently, EXAFS spectra collected on PSII samples in the S_3 state are especially susceptible to radiation-induced modifications.

The cystallographically determined electron densities correspond to a situation where mostly Mn^{II} is present [37–39]. The Mn–Mn or Mn–Ca distance are no longer detectable by EXAFS because either these distances exceed ∼3.5 Å or the distance heterogeneity is so pronounced that all shorter Mn–Mn and Mn–Ca distances become EXAFS-invisible. The EXAFS data does not allow for any statement whether the positions of the ligating

amino acids are affected by reduction of the Mn ions. At an advanced state of X-ray damage, large-scale structural changes affect the size of the unit cell of protein crystals and eventually result in a loss of diffraction reflexes [201,202]. We note that the X-ray photoreduction of the Mn complex clearly precedes these drastic effects. For assessment of the reliability of the crystallographic data on the Mn–ligand environment, it will be crucial to determine to what extent – at cryogenic temperatures, but in the 'energized situation' created by X-ray exposure – the Mn reduction can initiate distinct movements of the ligating amino-acid residues.

In conclusion, the crystallographic data refers to an all-Mn^{II} complex rapidly formed also at low temperatures by X-ray irradiation. The resolution of electron density assignable to ligating amino acids suggests that the described Mn photoreduction does not result in a highly disordered situation, with the possible exception of the environment of the Mn ion closest to Asp 170 [26]. Complete avoidance of X-ray photoreduction in the course of the crystallographic data collection represents an enormous difficulty as it would require a decrease in dose by several orders of magnitude.

3.2.2. Structure in the dark-stable S_1-state

Mostly on the basis of EXAFS results, the group of Klein et al. suggested the presence of two di-μ_2-oxo bridged Mn dimers (2× Mn–Mn distances of 2.7 Å) which are connected by a mono-μ-oxo, bis-carboxylato bridge (Mn–Mn distance of 3.3 Å) such that a C-shaped structure resulted [167]. This "dimer-of-dimers model" was used in formulation of numerous mechanistic models. For example, in the hydrogen-atom abstraction model [78,79] the O–O bond is formed between two oxo groups coordinated to the outer Mn ions, which were calculated on the basis of the dimer-of-dimers model and polarized EXAFS data [204] to be at an appropriate distance. Extensive simulations of EPR spectra led to the suggestion of a modification towards a trimer–monomer (or dangler) model [52,175]. Also the crystallographic results [23–26] are difficult to reconcile with a C-shaped dimer-of-dimers model, though specific isomers of the dimer-of-dimers model might be compatible [44,204].

In 2004, Barber and coworker presented a crystallographic model involving a $Mn_3Ca(\mu_3\text{-}O)_4$ cubane with the fourth Mn ion connected by a bridging oxide to the cubane [25]. This model has been used as a starting point for DFT calculations [106] and mechanistic considerations [6,105,106,205]. However, without modifications the model of Barber and coworkers is difficult to reconcile with the EXAFS results [37,46]. Quantum chemical studies of Batista and coworkers suggest moderate modifications of the model proposed by Barber and coworkers; the resulting structure may be compatible also with EXAFS results [61,206].

Recently, XAS data was collected in a pioneering experiment on single crystals of PSII [46], thereby providing further constraints for structural models of the Mn complex which complement earlier results obtained by XAS on isotropical [40,42,170,171,197,199,207] and uni-directionally oriented PSII samples [37,40,168,203,208,209]. The symmetry properties of the PSII crystals render interpretation of the single-crystal EXAFS in terms of structural models challenging. From the $P2_12_12_1$ crystal-symmetry and the non-crystallographic, local C2 symmetry result eight orientations of each vector connecting, e.g., two distinct Mn ions. Therefore unique structural information cannot be deduced directly from the single-crystal EXAFS data. Comparison of the single-crystal EXAFS, crystallographic and other results with an extended set of hypothetical structures has lead Yano et al. to a stimulating novel hypothesis on structure and orientation of the $Mn_4Ca(\mu\text{-}O)_n$ core of the Mn complex; at this stage, a definitive assignment of the ligating amino-acid residues has not been possible [46].

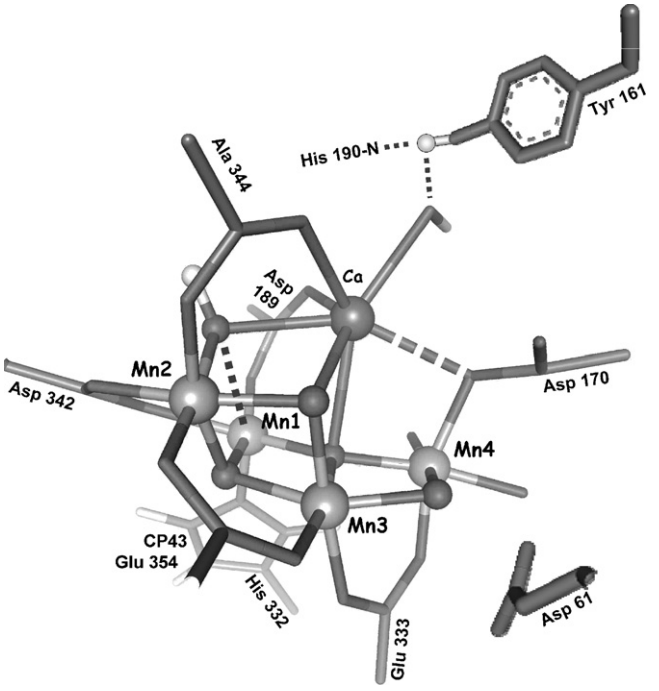

Fig. 10. Tentative model of the Mn complex in its S_1-state. The ligation of the metal ions by amino acid residues is in accord with the crystallographic model of [26]. The μ-oxo bridging between metal ions was chosen such that the final model (i) matched the EXAFS results obtained on isotropic and uni-directionally oriented PSII samples and (ii) could account in a straightforward way for structural changes in the S-state cycle. Molecular mechanics modeling was employed where a standard force-field had been complemented by reasonable constraints for the Mn–ligand distances and Mn–Mn distances. Starting with the coordinates of [26], minimization of the potential energy was carried out by allowing for changes in the coordinates of atoms within a narrow range around Mn1, Mn2, and Mn3, but within a clearly extended range around Mn4, to account for the putative influence of radiation-induced modifications on Mn4 and its ligand environment. In the shown model, Mn1 and Mn2 are close to the original coordinates of [26]; Mn3 is moderately shifted, but the positions of Mn4 and the Asp_{170} deviate clearly from the initial model [26]. The $S_0 \rightarrow S_1$ transition is supposed to involve deprotonation of the μ_2-oxo bridge between Mn3 and Mn4. Up to the S_2-state, the hydroxide bridging between Mn2 and Ca is only loosely ligated to Mn1 (Mn1–O distance > 2.4 Å). In the $S_2 \rightarrow S_3$ transition, the five-coordinated Mn1 is oxidized and transformed into a six-coordinated Mn^{IV}, a process associated with deprotonation and proton release. In the thereby formed S_3-state complex, a $Mn_3Ca(\mu\text{-}O)_4$ cubane is present. The model implies that the substrate-water molecules bind at or close Mn4 because (i) only Mn 4 is coordinatively not fully saturated by μ-oxo and amino-acid ligands and (ii) there is sufficient space around Mn4 to account for several water molecules. For further details, see [210].

Further structural models need to be discussed and evaluated in the light of all available experimental (and theoretical) evidence, in order to advance towards a definitive and complete (with respect to the Mn–ligands) atomic-resolution model. A tentative model [210], which involves a structural motif *not* considered in [46], is shown in Fig. 10.

3.2.3. Oxidation-state assignment in the S_1-state

In 1981, Dismukes and Siderer described a multiline EPR signal present only in the S_2-state of the Mn complex which exhibits striking similarities to the 16-line signal of binuclear $Mn_2^{III,IV}$-complexes [211]. Today it is commonly believed that either a tetranuclear $Mn_4^{III,III,III,IV}$ or $Mn_4^{III,IV,IV,IV}$ complex gives rise to this multiline EPR signal [52,53,173]. Arguments in favor of the low-valence oxidation-state combination (III,III,III,IV) have been presented [53,212], but the evidence in favor of the high-valence combination (III,IV,IV,IV) seems to be clearly stronger. All involved XAS groups have concluded that the XANES spectra essentially exclude oxidation states of $Mn_4^{III,III,III,III}$ and $Mn_4^{III,III,III,IV}$ in the S_1 and S_2 state, respectively [40,197,213] (Figs. 11 and 12). Also recent computational analyses of EPR data favors the high-valence state [52,173]. Oxidation of the Mn complex by electron removal from a delocalized orbital has been proposed [214], but interpretation of the data obtained by the promising new RIXS method is still in its infancy. It is commonly believed that the $S_1 \rightarrow S_2$ transition involves oxidation of a distinct Mn ion from the Mn^{III} to the Mn^{IV} level. Thus in the S_1-state the oxidation-state combination of the four Mn ions likely is III,III,IV,IV.

3.2.4. The $S_0 \rightarrow S_1$ transition

In the $S_0 \rightarrow S_1$ transition, one-electron Mn oxidation is suggested by the observed X-ray edge shift [40,44,215–218] (Fig. 11). Assuming localized valence states, there are the alternative options of either $Mn^{II \rightarrow III}$ or $Mn^{III \rightarrow IV}$ oxidation. In [216] we suggested that a shoulder in the edge spectra could point towards the presence of Mn^{II} in the S_0-state, because similar shoulders were observed in PSII preparations contaminated by spurious Mn^{II}. In the meantime a better understanding of the factors that determine the shape of X-ray edge spectra has been obtained [44]. By ab-initio XANES simulation we recently found that, for axially Jahn–Teller elongated Mn–ligand distances of the Mn^{III} ion, a $Mn^{III \rightarrow IV}$ transition can account in a more straightforward way for the observed S_0-S_1 difference spectrum than a $Mn^{II \rightarrow III}$ transition [44,219–221]. The presence of one Mn^{II} ion in the S_0-state complex also had been concluded from the width of the S_0-state EPR signal [222,223]. However, in a more recent EPR analysis evidence was presented that Mn^{II} is not present [173]. In conclusion, the balance of evidence is leaning towards a $Mn_4^{III,III,III,IV}$ complex in the S_0 state, but definitive proof is still lacking.

For investigation of the S_0 state, EXAFS spectra were collected at 20 K after illumination with three Laser-flashes at room temperature and subsequent freezing in liquid nitrogen (flash-and-freeze approach) [40,145]. In another set of experiments, the flash-illumination was directly combined with XAS

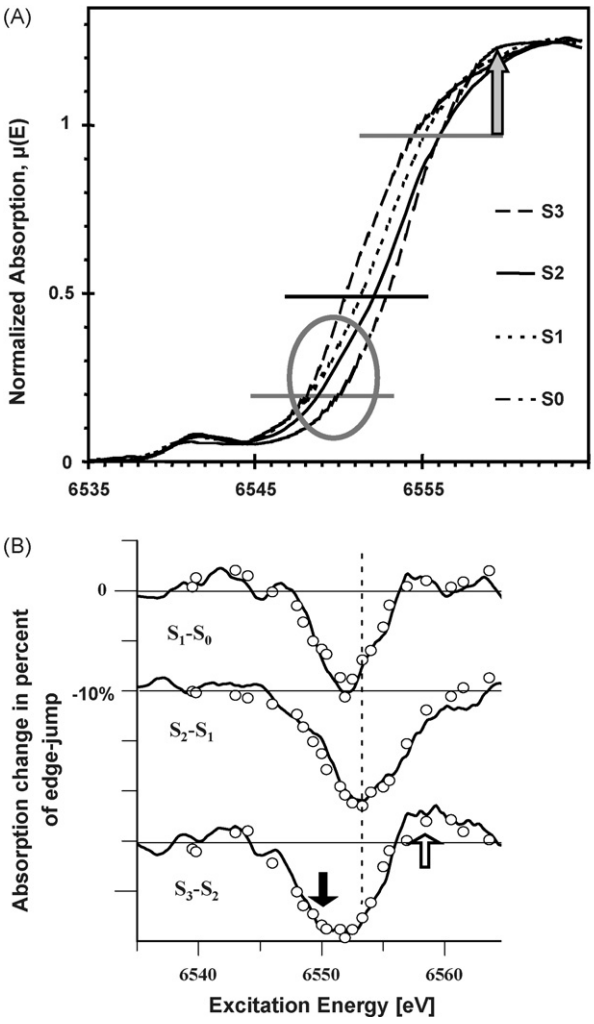

Fig. 11. Mn K-edge spectra of the Mn complex for all four semi-stable S-states (modified from [145]). (A) Data collected at 20 K; (B) comparison of difference spectra collected at room temperature and 20 K. In all S-state transitions the position of the X-ray edge overall shifts to higher energies, but a uniform edge-shift is not observed. In the rising part of the X-ray edge, the shift of the X-ray edge in the $S_2 \rightarrow S_3$ transition is particularly pronounced (bottom grey line in A), whereas towards the maximum of the X-ray edge no shift towards higher energies is observed (top grey line in A). At the half-height off the normalized spectra, all oxidizing S-state transitions results in approximately the same edge-shift. The grey oval (in A) highlights the especially pronounced absorption decrease in the $S_2 \rightarrow S_3$ transition observed below 6550 eV, which relates to disappearance of a shoulder present in the S_2 state spectrum. In (A), the grey arrow highlights a remarkable absorption increase at ~6559 eV which is associated with the $S_2 \rightarrow S_3$ transition; the same absorption increase is marked in the difference spectrum in B by an unfilled arrow.

at room temperature using either a rapid-scan or a timescan approach [93,94]. Furthermore, XAS data was collected at 20 K on S_0-state samples prepared by a protocol involving Laser-flash illumination and an external reductant [146]. Consistently it is found that, in comparison to the S_1-state, the Fourier-transformed EXAFS spectra are characterized by a reduced magnitude of the first and, especially, the second Fourier peak (Fig. 13). The first-peak magnitude increases with increasingly homogenous Mn–ligand distances. It is maximal in the S_3-state, where minimal distance heterogeneity is explainable by four

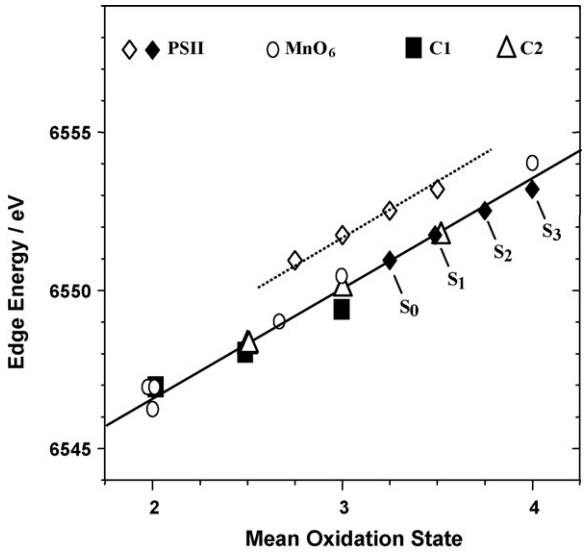

Fig. 12. Comparison of the Mn K-edge energies of the four S-states with those of Mn oxides [44] and of two binuclear Mn compounds in different oxidation states [180]. The edge energies have been determined by the "integral method" described in [44]. For the high-valence scenario (solid diamonds), the edge energies of the S-states are compatible with the oxidation-state dependence of the edge energy observed in the reference compounds. For the low-valence attribution to the S-states of PSII (open diamonds), significant deviations are observed, rendering the low-valence option unlikely.

hexa-coordianted Mn ion with identical oxidation state (Mn^{IV}) [40,145]. In the S_0-state, the first-peak magnitude is minimal suggesting a maximal distance heterogeneity. This is explainable by the presence of several Mn^{III} ions in a Jahn-Teller distorted geometry.

From simulation of the EXAFS oscillations it is proposed that, in comparison to the S_1 state, the low second-peak magnitude in the S_0 state (Fig. 13) is explainable by the presence of a ~2.8 Å Mn–Mn vector in the S_0 state which is transformed to a ~2.7 Å Mn–Mn vector in the $S_0 \rightarrow S_1$ transition [40,145]. The transition from a Mn^{IV}(μ-O)(μ-OH)-Mn^{III} to a Mn^{IV}-(μ-O)$_2$-Mn^{IV} motif could explain the distance decrease from 2.7 to 2.8 Å straightforwardly [224], but also more complex structural changes might be involved.

3.2.5. The $S_1 \rightarrow S_2$ transition

The X-ray edge shift by at least 0.7 V to higher energies [45,145,215,216,218,225] (Figs. 11 and 12) leads to the supposition of a one-electron oxidation of manganese in the $S_1 \rightarrow S_2$ transition, most likely from the $Mn_4^{III,III,IV,IV}$ to the $Mn_4^{III,IV,IV,IV}$ level (see Section 3.2.3). This transition most likely is *not* associated with deprotonation of the Mn complex (Section 2.3.1) pointing towards mere Mn oxidation without any associated chemical change. This conjecture is supported by the EXAFS analysis which does not provide any indications for changes in the bridging between Mn ions, as opposed to all other transitions between semi-stable S-states. In conclusion, the available experimental results consistently suggests that the $S_1 \rightarrow S_2$ transition is exceptional as it is the only transition between semi-stable S-states which does not involve chemical changes and proton release.

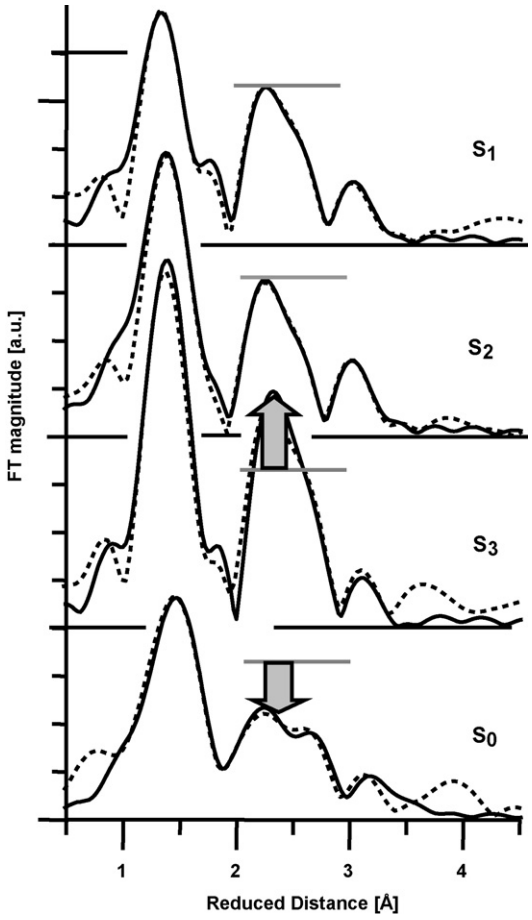

Fig. 13. Fourier-transformed EXAFS spectra of the Mn complex in the four semi-stable S-states (at 20 K). Solid lines represent simulations of the experimental spectra (dotted lines). The second Fourier peak originates from Mn–Mn vectors of ~2.7 Å length assignable to Mn–(μ-O)$_2$–Mn motifs. The arrow indicates the increase (in the S_3-state) or decrease (in the S_0 state) in the magnitude of the second Fourier peak relative to the level in the S_1 and S_2 state (grey line) (modified from [145]).

3.2.6. The $S_2 \rightarrow S_3$ transition

This transition between semi-stable S-states requires a more extended discussion because several principal aspects are still under debate.

3.2.6.1. Mn versus ligand oxidation. Whereas for the $S_0 \rightarrow S_1$ and $S_1 \rightarrow S_2$ transitions, oxidation of a Mn ion is generally assumed, the localization of the oxidizing equivalent created in the $S_2 \rightarrow S_3$ transition is still debated. The following alternatives have been discussed (for details see [40,42]): (i) Mn-centered oxidation, most likely a $Mn^{III \rightarrow IV}$ oxidation; (ii) radical formation by oxidation of a ligating amino-acid residue, e.g. a histidine [226]; (iii) formation of an oxygen radical ($O^{\bullet}$ or $OH^{\bullet}$) on a direct Mn–ligand, possibly being a partially oxidized water molecule in bridging position between Mn ions [41,196,197]; (iv) delocalization of the oxidation equivalent (delocalized valence orbital and spin densities; delocalized versus trapped valencies).

A delocalized valence orbital has been suggested [214], but would be untypical for $Mn^{III/IV}$-oxo complexes and presently

is not strongly supported by experimental results. The formation of a histidine radical had been proposed (option ii), mostly on the basis of an EPR signal detected in Ca-depleted PSII [226], but in subsequent studies an alternative explanation of the experimental observations has been suggested [227].

Today mostly the options (i) and (iii) are discussed. Their discrimination is of importance with respect to the general mechanism of photosynthetic water oxidation. Mn-centered oxidation on all S-state transitions would support the original hypothesis of Kok that the onset of water oxidation is delayed until four oxidizing equivalent have been accumulated by the 'catalyst' [87], whereas oxidation of an oxygen ligand could indicate partial water oxidation at an earlier stage in the reaction cycle.

From computational chemistry the formal Mn oxidation state of Mn in multinuclear complexes is *not* closely related to the Mulliken charge of the Mn ion; however, a good correlation with the spin-population on the respective Mn ion is observed [61,228]. Thus, in contrast to other transition metal ions, the assumption of localized, integer oxidation states is not unreasonable for Mn complexes. An often useful criterion for a distinct Mn oxidation state is (i) the Mn–ligand bond length which, for unchanged coordination number, decreases with increasing oxidation state (bond-valence rules, see [229–231]), as well as (ii) the presence of a Jahn–Teller distortion in the Mn^{III}-state. The correlation between oxidation state and bond length also is related to the empirically observed shift of the X-ray edge position to higher energies upon oxidation of manganese (see Fig. 12). For a more comprehensive discussion, see [42].

To study Mn oxidation state changes, XANES spectra were collected at the Mn K-edge. The changes in the edge spectra (Fig. 11) have been interpreted as evidence either for [145,215,216] or against [217,218] manganese-centered oxidation in the $S_2 \rightarrow S_3$ transition. Comparison of the S_3-S_2 difference spectra presented in [218] (absence of Mn-centered oxidation concluded) and [145] (Mn oxidation proposed) reveals only minor differences in the data itself. Why does the interpretation differ so pronouncedly?

In all S-state transitions, the X-ray edge does not shift uniformly to higher energies but also changes its shape, especially in the $S_2 \rightarrow S_3$ transition. Therefore the edge-shift depends on the method used for quantification of X-ray edge positions. The inflection-point energy (IPE, determined as the zero-crossing energy of the second derivative) as used in [217,218] is particularly shape-sensitive and may be generally inappropriate in investigations on multinuclear metal centers with localized valencies; for a detailed account, see [42]. The "integral method" described in [42] seems to be more appropriate, however casting the complex XANES changes into a single number remains critical.

First steps to interpret changes in the XANES spectra upon advancement in the S-state cycle in terms of changes in the electronic and geometric structure of the metal complex have lead to the proposal that the $S_2 \rightarrow S_3$ transition involves transformation of five-coordinated Mn^{III} into six-coordinated Mn^{IV} [42,219,221]. This assumption can explain the observed

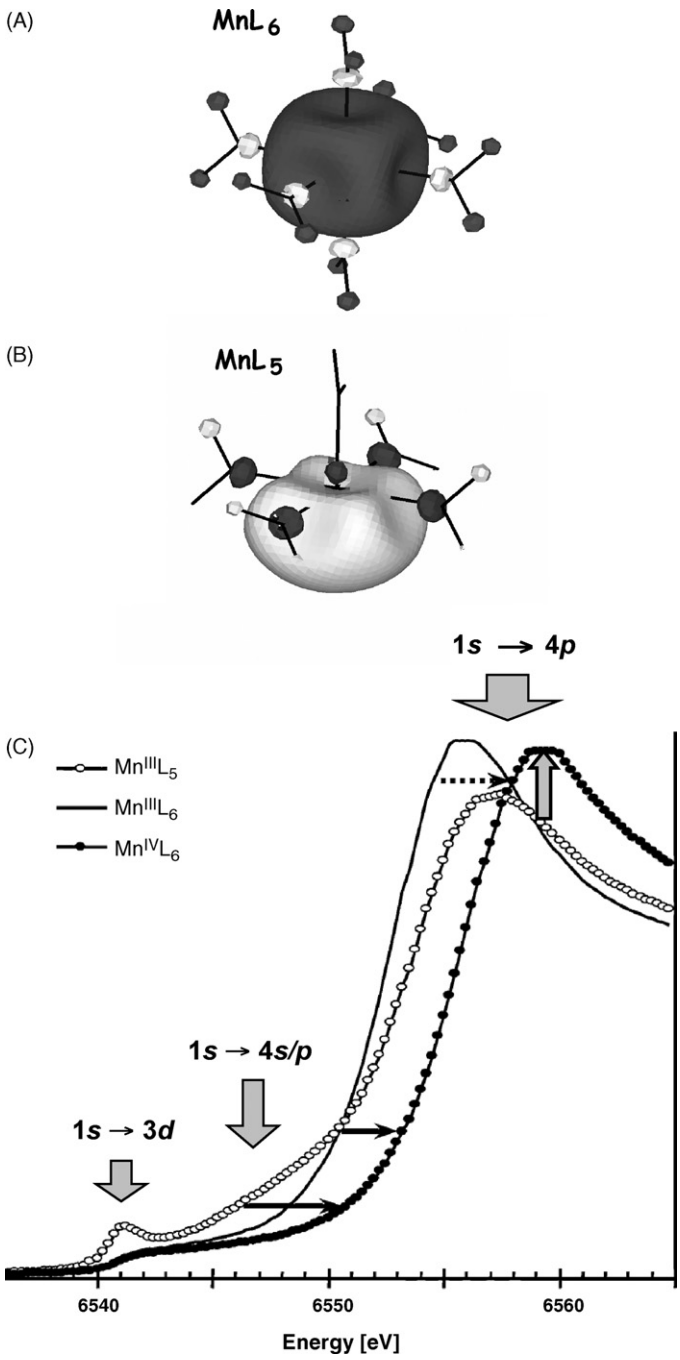

Fig. 14. Qualitative molecular-orbital calculations (A) and XANES simulations (B) addressing the edge-shape changes in the $S_2 \rightarrow S_3$ transitions. (A) Selected molecular orbitals of six-coordinated and five-coordinated manganese symmetrically coordinated by water molecules. Both orbitals are dominated by the Mn 4s contributions. In the six-coodinated complex (of idealized octahedral geometry) there is no contribution of the Mn 4p orbital, whereas in the five-coordinated complex significant p-orbital contributions are present. Consequently the formally dipole-forbidden 1s → 4s transition becomes partially dipole-allowed in the five-coordinated complex and thus visible in the K-edge spectrum; for details see [44]. (B) XANES spectra simulated for five- and six-coordinated Mn(III), and for six-coordinated Mn(IV) in idealized ligand geometry. Open circles: $Mn^{III}(H_2O)_2(OH)_3$, Mn–O distance of 1.95 Å, square-pyramidal geometry. Solid line: $Mn^{III}(H_2O)_3(OH)_3$, Mn–O distance of 2.02 Å, octahedral geometry. Filled circles: $Mn^{IV}(H_2O)_2(OH)_4$, Mn–O distance of 1.90 Å, octahedral geometry. The prevailing electronic transitions which dominate in the respective edge regions are indicated (modified from [219]).

edge-shape changes qualitatively [42,219] (see Fig. 14) and quantitatively [220,221] in a straightforward way. Ab-initio XANES simulations [232] for a numerical model of water oxidation involving $(\mu\text{-O})^{\bullet}$ formation in the $S_2 \rightarrow S_3$ transition [233,234] (atomic coordinates kindly provided by P.E.M. Siegbahn, Lund), results in S_3–S_2 difference spectra which differ qualitatively from the experimental results [221]. How a change from five-coordinated Mn^{III} to six-coordinated Mn^{IV} would affect the spectrum of the k_β X-ray fluorescence, which also has been studied for PSII in various S-states [218], is unknown. In conclusion, the edge-shifts and shape changes in the $S_2 \rightarrow S_3$ transition are compatible with a $Mn^{III}L_5 \rightarrow Mn^{IV}L_6$ transition (option (i)), but are difficult to reconcile with formation of a ligand radical (options (ii) and (iii)). We note that, to account for the XANES changes, the $Mn^{III}L_5$ ion in the S_2-state does not need to be strictly five-coordinated but could have a sixth ligand at a distance exceeding 2.4 Å.

3.2.6.2. Structure and valence localization at room temperature. Inter alia to address the question whether potentially conflicting results on the S_3-state relate to a temperature-dependent localization of oxidizing equivalents (redox isomerism) or protonation states, we investigated the Mn complex by XAS at room temperature [91–94,145] and approached a comparison to results obtained at 20 K. In a recent especially comprehensive study [145], for each of the four semistable S-states, XANES and EXAFS spectra were collected at 20 K as well as at room temperature and jointly evaluated with focus on the structural changes in the S-state cycle (Fig. 15). Any oxidation-state and structural modifications by X-ray irradiation were excluded by strictly limiting the maximal dose, as documented for each S-state in the supporting online material of [145].

No indications for temperature-dependent equilibria were obtained [145]. The XANES spectra measured at room temperature and 20 K are virtually identical (Fig. 11). The 20 K and room-temperature EXAFS spectra differ in the magnitude of the EXAFS oscillations at higher energies, but only because thermally activated (vibrational) motions increase the distance spread at room temperature (increased Debye–Waller parameter σ). Otherwise, essentially identical structural parameters were determined by simulation of EXAFS spectra collected at room temperature (RT) and at 20 K, for each semi-stable S-state [145].

3.2.6.3. Structural changes. In the $S_2 \rightarrow S_3$ transition, we consistently have observed an increase in the first and second Fourier-peak in all data sets collected at room temperature and at 20 K [40,92,145] (Fig. 13). Furthermore, the corresponding increase in the EXAFS oscillations becomes directly visible in the time courses of the flash-induced changes in the X-ray absorption when the advancement in the S-state cycle is measured at room temperature in 'real time' [145]. In [235] a pronounced decrease in the magnitude of the EXAFS oscillations, and consequently of the first and second Fourier-peak, has been reported; the reasons for this deviating observation are still unclear.

The EXAFS simulations indicate that the increase in the second Fourier peak originates from an increased number of

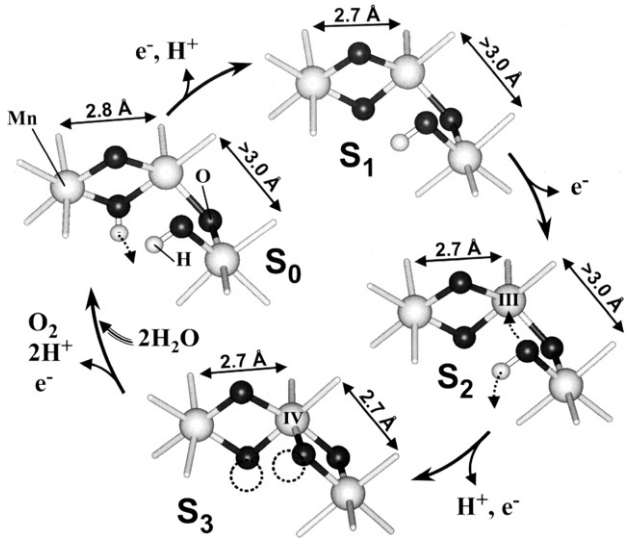

Fig. 15. Structural changes in the μ-oxo core of the Mn complex. For clarity, only three Mn ions of the Mn_4Ca-complex are shown which suffices to illustrate the putative modifications in the structure of the complex. The Mn–Mn distances derived from the EXAFS are indicated. The omitted fourth Mn is assumed to be connected to one of the depicted Mn ions by a di-μ-oxo bridge leading to a further Mn–Mn vector of ~2.7 Å (in all S-states). One Ca ion (not shown) presumably is connected by two or more bridging oxygen atoms (μ-O, μ-OH, $\mu\text{-OH}_2$) to two or more Mn ions. Alternatively to the depicted Mn-$(\mu_2\text{-O})_2$-Mn-$(\mu_2\text{-O})$-Mn motif in the S_1-complex, a $Mn_3(\mu_2\text{-O})(\mu_3\text{-O})$ motif might be present which then is transformed to a $Mn_3(\mu_2\text{-O})_2(\mu_3\text{-O})$ unit in the $S_2 \rightarrow S_3$ transition. Single-electron oxidation of manganese is assumed to occur on $S_0 \rightarrow S_1$, $S_1 \rightarrow S_2$, and $S_2 \rightarrow S_3$, but only the oxidation state of the five-coordinated Mn^{III} (in S_2) which is transformed into a six-coordinated Mn^{IV} (in S_3) is indicated. Ligand deprotonation and rearrangement presumably taking place in the subsequent S-state transition are emphasized using dotted arrows. In S_3, dotted circles mark the sites where bridging oxides may act as proton acceptors in $S_3 \Rightarrow S_0$, the oxygen-evolution transition (from [145]).

Mn–Mn vectors in the distance range from 2.7 to 2.8 Å [40,145]. This observation is explainable by formation of an additional di-μ-oxo motif in the $S_2 \rightarrow S_3$ transition (Fig. 15) [40,145].

In summary, we propose that in the $S_2 \rightarrow S_3$ transition the transformation of a five-coordinated Mn^{III} to a six-coordinated Mn^{IV} is coupled to the formation of an additional μ-oxo bridge. This process is preceded (or coupled to) a deprotonation, possibly of a terminally coordinated water species which turns into a bridging oxide or hydroxide. The experimentally determined exchange rates for the two substrate-water molecules do not vary strongly when comparing the states S_2 and S_3 [59,236], suggesting that the formed μ-oxo bridge is not derived from a substrate-water molecule.

3.2.7. Four steps of the $S_3 \rightarrow S_0$ transition

In the $S_3 \rightarrow S_0$ transition, clearly dioxygen and likely two protons are released from the Mn complex (see Section 2.3); at least one and supposedly both of the substrate-water molecules for the next turnover of the catalytic cycle bind [54,59,60,236–238]. In Fig. 5 (Eqs. (7)–(9) and (1)), these events are described by a sequence of four reactions: S_3^+ (the classical S_3) $\rightarrow S_3^n$ (S_4 in [95]) $\rightarrow S_4^+ \rightarrow S_0^+ \rightarrow S_0^n$ (the classical S_0), where only the S_4^n may represent a transition-state-like intermediate.

3.2.7.1. Deprotonation prior to ET to $Y_Z^{\bullet+}$ ($S_3^+ \rightarrow S_3^n$). Evidence has been presented that the $Y_Z^{\bullet+}$-formation may induce a deprotonation of the Mn complex ($S_3 \rightarrow S_4$ in [95], see Section 2.2). There are three mechanistically distinct alternatives for the identity of the deprotonating group:

(i) A substrate-water molecule is directly deprotonated.
(ii) The substrate water is not deprotonated, but a base is created by deprotonation of a first-sphere Mn–ligand, e.g. a μ-OH group. In the dioxygen formation reaction itself, this base could facilitate a coupled electron–proton transfer from substrate water to the core of the Mn complex, in analogy to the proposed role for the deprotonated μ-oxo bridges formed in the $S_0 \rightarrow S_1$ and $S_2 \rightarrow S_3$ transition [40,165].
(iii) A nearby group, e.g. the Arg_{357} of the CP43 protein [106,107], is deprotonated and then accepts a proton in the subsequent steps of dioxygen formation.

A high-valent S_3 state (all-Mn^{IV}) may be incompatible with the presence of a protonated oxo-bridge, thereby disfavoring hydroxo-bridge deprotonation in the $S_3^+ \rightarrow S_3^n$ transition. For substrate water coordinated to the Mn ion closest to Asp_{61} (Mn4 in Fig. 10), its deprotonation may be disfavored by the relatively large distance to $Y_Z^{\bullet+}$ (in comparison to Mn1 and Mn2); the through-space and through-bond interactions could be too weak for hydroxide formation. Be that as it may, presently it is not possible to exclude – or even disfavor – any of the above alternatives on solid grounds.

3.2.7.2. Electron-transfer to $Y_Z^{\bullet+}$ ($S_3^n \rightarrow S_4^+$). This electron-transfer step is proposed to be facilitated by the potential-lowering effect of the preceding deprotonation [95,96]. The sequence of deprotonation and ET may be similar to the $S_2 \rightarrow S_3$ transition, however the energetic constraints differ. In the $S_3^n \rightarrow S_4^+$ transition, the electron transfer does not result in formation of a semi-stable state so that the ET-step also could be endergonic. Thus the S_4^+/S_3^n redox potential could exceed the $Y_Z^{\bullet+}/Y_Z$ potential (~1.1 V) maximally by the activation energy (in V) of the ms-rate constant of the $S_3^n \rightarrow S_4^+ \rightarrow S_0^+$ transition (~0.2 eV) [99,130,137,154] resulting in a maximal potential of ~1.3 V versus ~1.05 V for the other S_{i+1}^+/S_i^n couples. If the S_4^+/S_3^n potential is close to 1.3 V, then (a) the potential-lowering influences of the preceding deprotonation will be relatively small (favoring the third of the above options for the deprotonation in $S_3^+ \rightarrow S_3^n$) and (b) the S_4^+ state will be particularly strongly oxidizing.

Application of standard rules-of-thumb for biological electron transfer [239] suggests for a donor-acceptor distance of less than 7 Å (Y_Z to nearest Mn ion) and an activation energy of only ~0.2 eV that the ET rate constant should be several orders of magnitude greater than the experimentally determined value of ~0.7 ms^{-1}. (Noteworthy, also the ET rates in the transitions $S_0^n \rightarrow S_1^+$ and $S_1^n \rightarrow S_2^+$ are surprisingly low.) This discrepancy is not easily explainable by rate-limitation by a coupled proton-tunneling process because the H/D isotope effect on the rate is small (≤1.4). Protein dynamics involving diffusive motions between numerous conformational substates [240–243] or specific, 'conducive' protein motions [244,245] may facilitate a significant reorganization of the Mn complex – including proton movements – at low activation enthalpy. We note that such an influence of the protein dynamics could render quantum chemical calculations on the energy profile along putative reaction paths problematic. Whether the slowed-down ET in PSII in which Sr replaces Ca relates to protein dynamics or rather changes in the energetics (redox potentials, p*K*-values) is still unclear; the latter may be more likely [102,246]. It will be important to address these and related questions in the future.

3.2.7.3. Mn reduction coupled to dioxygen formation ($S_4^+ \rightarrow S_0^+$). The chemical changes of the oxidizing S-state transitions are necessarily reversed in the $S_3 \rightarrow S_0$ transition (assuming that the two substrate water molecules are already bound in the semi-stable S_0-state). Thus, on the basis of the results summarized above, we suggest that in the $S_4^+ \rightarrow S_0^+$ transition, the Mn reduction to the $Mn^{III,III,III,IV}$ level is accompanied by changes in the Mn–Mn bridging mode, namely (i) a $Mn_2(\mu\text{-}O)_2 \rightarrow Mn_2(\mu\text{-}O)(\mu\text{-}OH)$ and (ii) $Mn_2(\mu\text{-}O)_2 \rightarrow Mn_2(\mu\text{-}O)_1$ transition, where the latter involves a $Mn^{IV}L_6 \rightarrow Mn^{III}L_5$ coordination change (Fig. 15). We feel that more far-reaching hypotheses on the atomic-level events in this crucial reaction step cannot be derived directly from the presently available experimental results. A more general hypothesis on the basic mechanism of dioxygen formation in the $S_4^+ \rightarrow S_0^+$ transition is discussed below (see Section 3.3).

3.2.7.4. Proton release prior to S_0-formation ($S_0^+ \rightarrow S_0^n$). This proton release may be coupled to the structural reorganization that is associated with dioxygen release and the binding of another set of substrate-water molecules. Three alternatives may be distinguished: (i) a substrate-water molecule binds to a Mn or Ca ion and deprotonates, resulting in formation of a bound hydroxide. (ii) Concomitantly to Mn reduction in the $S_4^+ \rightarrow S_0^+$ step, a first-sphere ligand (e.g. a μ-oxo bridge) became protonated and now deprotonates. (iii) A nearby group (e.g. Asp_{61}, Arg_{357}, non-substrate water) accepted a proton in the $S_4^+ \rightarrow S_0^+$ transition and now releases the proton into the lumenal bulk phase. The first option amounts to binding of one substrate water in form of a hydroxide. It is doubtful whether a hydroxide coordinated to a high-valent Mn ion exchanges as fast as experimentally observed (exchange in ~500 ms in the S_3 state [59,60,237] where, supposedly, four Mn^{IV} ions are present). Nonetheless, presently none of the above alternatives can be excluded.

3.3. Acceptor-base hypothesis—an alternative mechanistic framework

In the light of the considerations and experimental observations reviewed above, we propose the following framework model for the mechanism of photosynthetic water oxidation at the Mn complex of PSII:

(1) By electron transfer to $Y_Z^{\bullet+}$ and proton release into the aqueous bulk phase, four electrons and four protons are alternately removed from the Mn complex as shown in Fig. 5. The interlaced deprotonation steps facilitate an almost constant redox potential of the Mn complex in four successive oxidation steps and simultaneously ensure minimal free-energy losses. The latter requires that the four ET steps proceed at a redox potential close to 1.05 V whereas the deprotonation steps are characterized by a p*K* close to 4.5. (The p*K* of the deprotonating group will change in subsequent oxidation steps, but this is not associated with a loss in the free-energy available for the elementary steps of dioxygen formation.)

(2) Water is neither partially oxidized nor deprotonated in the oxidizing S-state transitions. Thus, four oxidizing equivalents as well as four bases are accumulated by the Mn complex before onset of water deprotonation and oxidation.

(3) In the reaction step(s) of O–O bond formation and dioxygen release (i.e. $S_3^n \rightarrow S_4^+ \rightarrow S_0^+$), the previously formed bases accept protons form the substrate-water molecules. Several or all of the acceptor bases are first-shell ligands of the Mn complex thereby facilitating a close coupling of the electron transfer from water to Mn ions (Mn reduction) and of protons to the Mn–ligands formally amounting to a hydrogen-atom transfer from water to the core of the Mn complex.

The hypothesis of Kok that four oxidizing equivalents are accumulated prior to the onset of water oxidation is, in the above framework model, extended by proposing that also four bases are accumulated by the catalyst—prior to oxidation and deprotonation of water.

Already Krishtalik has suggested that one or more bases created in the oxidizing S-state transitions could serve as proton acceptors in the dioxygen-formation step [161–164]. This idea repeatedly has been invoked in the interpretation of proton-release data [116,117].

The above framework model represents a working hypothesis which may or may not turn out to be too extreme in the assumption that *all* four protons are still bound to the two substrate-oxygen atoms in the S_4^+ state. Specifically the $S_3^n \rightarrow S_4^+$ and the $S_0^+ \rightarrow S_0^n$ transitions presumably involve more extensive structural rearrangements which likely include internal proton movements and *might* include deprotonation of a substrate-water molecule.

With respect to the above point (ii), we note that overall there is reasonably good evidence for the absence of partial water oxidation prior to formation of the S_4-state (S_3^n in Fig. 5); only for the $S_2 \rightarrow S_3$ transition this question is still debated (see Section 3.2.6). The situation is less clear with respect to water deprotonation; some tentative conclusions can be drawn from the available experimental results:

(i) In the $S_1 \rightarrow S_2$ transition no proton is released from the Mn complex so that substrate-water deprotonation in this step is most unlikely (Section 2.3).

(ii) The observation of only minor changes in the exchange rates of both substrate-water molecules in the $S_2 \rightarrow S_3$ transition essentially excludes substrate-water deprotonation in this step [59,236]. In general, the exchange rates determined for the PSII manganese complex do not provide any conclusive evidence that a substrate-water molecule is deprotonated in any of the transitions from S_0 to S_3 [59,60,236–238,247,248].

(iii) The $S_0 \rightarrow S_1$ transition may results in a deprotonation of a μ-OH bridge (Section 3.2.4); a recent investigation on relevant synthetic model complexes suggests that the water exchange rates observed for the PSII manganese complex are incompatible with a substrate-water oxygen forming a μ-oxo bridge between Mn ions (at least up to the S_3-state) [249]. In conjunction these observations suggest that the formation of an unprotonated μ-oxo bridge in the $S_0 \rightarrow S_1$ transition by deprotonation of a μ-hydroxo derived from a substrate-water molecule is unlikely, thereby providing a circumstantial argument against substrate-water deprotonation in the $S_0 \rightarrow S_1$ transition.

We feel that, overall, the available experimental evidence points towards the absence of substrate-water deprotonation in any of the transitions from S_0^n to S_3^+. At present there is, to our best knowledge, no experimental observations favoring or disfavoring deprotonation of substrate-water molecules in the $S_0^+ \rightarrow S_0^n$ or $S_3^+ \rightarrow S_3^n$ transition.

Numerous mechanistic models of dioxygen formation have been proposed, ranging from basic, empirical models to detailed atomic-level scenarios. For a summary of 34 earlier models see [8]; for a recent discussion of selected atomic-level models, see [6]. In the vast majority of these models, the two water molecules are partially or fully deprotonated when four oxidizing equivalents have been accumulated in the S_4-state, at variance with our acceptor-base hypothesis. One of the rare examples of a mechanistic model in which substrate-water deprotonation takes place only after formation of the S_3-state recently has been presented by McEvoy and Brudvig [6,107].

4. Concluding remarks

Photosynthetic water oxidation at the Mn complex of PSII is still insufficiently, but already now by far better understood than, e.g., electrochemical water oxidation at electrode surfaces. The already reached level and future progress relates to a crucial methodical advantage in PSII research, namely the preparation of four semi-stable intermediates (S_1^n, S_2^n, S_3^+ and S_0^+) by light-flash application. However, taking into account the complexity of the four-electron/four-proton chemistry, characterization of the four semi-stable states may not suffice for construction of unambiguous mechanistic models. Employment of structure-sensitive methods in time-resolved experiments represents a major challenge, but could facilitate the characterization of further intermediates of the reaction cycle, specifically the transiently formed states S_0^+, S_2^n, S_3^n in Fig. 5. Whether S_4^+ is resolvable in time-resolved studies is doubtful, but not a-priori excluded. Furthermore, the preparation and stabiliza-

tion of these and other reaction intermediates (see [82,250,251] and refs. therein) at cryogenic temperatures may facilitate their characterization. Trapping and characterization of additional intermediates in the $S_3^n \rightarrow S_4^+ \rightarrow S_0^+$ step would be highly desirable—e.g. the possibly peroxidic intermediate suggested by experiments at high O_2 partial pressure [147,148].

What are the next steps?

(i) The here proposed basic sequence of four electron and four proton removal steps (Fig. 5) is, in several points, still hypothetical and requires further experimental support, specifically with respect to the not yet detected intermediates S_2^n and S_0^+.
(ii) Identification of the four deprotonation events as either substrate-water deprotonation or acceptor-base creation will be essential for establishment of a general framework for mechanistic models.
(iii) Fully unambiguous identification of the chemical identity of the acceptor bases represents an essential basis for a mechanistic model at the atomic level.
(iv) Quantitative determination of energetic parameters (redox potentials, p*K*-values, enthalpy change in the dioxgen-formation step) may, inter alia, provide the criteria needed for judging quality and relevance of quantum chemical calculations on the mechanism of dioxygen formation.
(v) Design and detailed functional characterization of synthetic catalysts which mimic distinct aspects of biological water oxidation will play a crucial role in evaluating mechanistic hypotheses on the individual steps of the water-oxidation cycle in PSII.
(vi) Structural models of the Mn complex in PSII have been presented, but these are neither definitive and nor complete (see Section 3.2). Simultaneously or in concert with (i)–(v), the development of atomic resolution models will advance, not only for the dark-stable S_1^n, but also for other intermediates in the reaction cycle of Fig. 5. Quantum chemical calculations are likely to play a crucial role in the development of complete atomic resolution models. To leave the realm of speculations, an effort is needed to interface more extensively computational and experimental approaches. This also needs to involve a critical assessment of the reliability of structural information obtained by protein crystallography and spectroscopic methods, on the one hand, and computational methods, on the other hand. Eventually these efforts should result in a complete picture of the active-site structure which includes the location and protonation states of substrate-water molecules and all nearby groups possibly involved in proton translocation.
(vii) On the basis of (i)–(vi), and specifically on the basis of complete structural models for the starting state (S_3^n) and final state (S_0^+), unambiguous determination of the reaction path in O–O bond formation may be attainable.

Acknowledgements

Financial support by the Deutsche Forschungsgemeinschaft (DFG, SFB 498) and the Bundesministerium für Bildung und Forschung (BMBF, grant 05KS1KEA/6 in the $BioH_2$ consortium) is gratefully acknowledged. The data related to Fig. 12 was collected at the XAFS beamline of the EMBL outstation at the DESY (Hamburg) and at the KMC1 beamline of the BESSY (Berlin); the synthetic complexes denoted as C1 and C2 have been synthesized in the framework of the Swedish Consortium of Artificial Photosynthesis and of the SOLAR-H project; these complexes have been investigated by XAFS in a cooperation involving Ann Magnuson, Magnus Anderlund, Stenbjoern Styring and others.

References

[1] J.H.A. Nugent, Biochim. Biophys. Acta 1503 (2001) 1.
[2] R.J. Debus, Biochim. Biophys. Acta 1102 (1992) 269.
[3] D. Ort, C.F. Yocum, Oxygenic Photosynthesis—The Light Reactions, vol. 10, Kluwer Academic Publisher, Dordrecht, 1996.
[4] B.A. Diner, F. Rappaport, Annu. Rev. Plant Biol. 53 (2002) 551.
[5] J. Barber, Quart. Rev. Biophys. 36 (2003) 71.
[6] J.P. McEvoy, G.W. Brudvig, Chem. Rev. 106 (2006) 4455.
[7] R.E. Blankenship, Molecular Mechanisms of Photosynthesis, Blackwell Science, Oxford, England, 2002.
[8] K. Bacon, Photosynthesis—Photobiochemistry and Photobiophysics, Kluwer Academic Publishers, Dordrecht, 2001.
[9] L. Hammarstrom, L. Sun, B. Akermark, S. Styring, Spectrochim. Acta A: Mol. Biomol. Spectrosc. 57 (2001) 2145.
[10] O. Kruse, J. Rupprecht, J.H. Mussgnug, G.C. Dismukes, B. Hankamer, Photochem. Photobiol. Sci. 4 (2005) 957.
[11] B. Esper, A. Badura, M. Rögner, Trends Plant Sci. 11 (2006) 543.
[12] N.S. Lewis, D.G. Nocera, Proc. Natl. Acad. Sci. U.S.A. 103 (2006) 15729.
[13] L. Sun, L. Hammarström, B. Åkermark, S. Styring, Chem. Soc. Rev. 30 (2001) 36.
[14] R.L. Burnap, Phys. Chem. Chem. Phys. 6 (2004) 4803.
[15] G.M. Ananyev, L. Zaltsman, C. Vasko, G.C. Dismukes, Biochim. Biophys. Acta 1503 (2001) 52.
[16] M. Barra, M. Haumann, P. Loja, R. Krivanek, A. Grundmeier, H. Dau, Biochemistry 45 (2006) 14523.
[17] H. Dau, J. Photochem. Photobiol. B 26 (1994) 3.
[18] E.M. Aro, M. Suorsa, A. Rokka, Y. Allahverdiyeva, V. Paakkarinen, A. Saleem, N. Battchikova, E. Rintamaki, J. Exp. Bot. 56 (2005) 347.
[19] E.M. Aro, I. Virgin, B. Andersson, Biochim. Biophys. Acta 1143 (1993) 113.
[20] N. Adir, H. Zer, S. Shochat, I. Ohad, Photosynth. Res. 76 (2003) 343.
[21] A. Krieger, A.W. Rutherford, I. Vass, E. Hideg, Biochemistry 37 (1998) 16262.
[22] I. Vass, S. Styring, T. Hundal, A. Koivuniemi, E. Aro, B. Andersson, Proc. Natl. Acad. Sci. U.S.A. 89 (1992) 1408.
[23] A. Zouni, H.T. Witt, J. Kern, P. Fromme, N. Krauss, W. Saenger, P. Orth, Nature 409 (2001) 739.
[24] N. Kamiya, J.-R. Shen, Proc. Natl. Acad. Sci. U.S.A. 100 (2003) 98.
[25] K.N. Ferreira, T.M. Iverson, K. Maghlaoui, J. Barber, S. Iwata, Science 303 (2004) 1831.
[26] B. Loll, J. Kern, W. Saenger, A. Zouni, J. Biesiadka, Nature 438 (2005) 1040.
[27] J. Kern, B. Loll, A. Zouni, W. Saenger, K.D. Irrgang, J. Biesiadka, Photosynth. Res. 84 (2005) 153.
[28] R.M. Cinco, K.L.M. Holman, J.H. Robblee, J. Yano, S.A. Pizarro, E. Bellacchio, K. Sauer, V.K. Yachandra, Biochemistry 41 (2002) 12928.
[29] R.M. Cinco, J.H. Robblee, J. Messinger, C. Fernandez, K.L.M. Holman, K. Sauer, V.K. Yachandra, Biochemistry 43 (2004) 13271.
[30] C. Müller, P. Liebisch, M. Barra, H. Dau, M. Haumann, Phys. Scripta T115 (2005) 847.
[31] M.J. Latimer, V.J. DeRose, I. Mukerji, V.K. Yachandra, K. Sauer, M.P. Klein, Biochemistry 34 (1995) 10898.
[32] K. Lindberg, L.E. Andreasson, Photosynth. Res. 34 (1992) 147.

[33] H. Wincencjusz, C.F. Yocum, H.J. van Gorkom, Biochemistry 37 (1998) 8595.
[34] K. Olesen, L.E. Andreasson, Biochemistry 42 (2003) 2025.
[35] P.O. Sandusky, C.F. Yocum, Biochim. Biophys. Acta 766 (1984) 603.
[36] M. Haumann, M. Barra, P. Loja, S. Löscher, R. Krivanek, A. Grundmeier, L.E. Andreasson, H. Dau, Biochemistry 45 (2006) 13101.
[37] H. Dau, P. Liebisch, M. Haumann, Phys. Chem. Chem. Phys. 6 (2004) 4781.
[38] J. Yano, J. Kern, K.-D. Irrgang, M.J. Latimer, U. Bergmann, P. Glatzel, Y. Pushkar, J. Biesiadka, B. Loll, K. Sauer, J. Messinger, A. Zouni, V.K. Yachandra, Proc. Natl. Acad. Sci. U.S.A. 102 (2005) 12047.
[39] M. Grabolle, M. Haumann, C. Muller, P. Liebisch, H. Dau, J. Biol. Chem. 281 (2006) 4580.
[40] H. Dau, L. Iuzzolino, J. Dittmer, Biochim. Biophys. Acta 1503 (2001) 24.
[41] J.H. Robblee, R.M. Cinco, V.K. Yachandra, Biochim. Biophys. Acta 1503 (2001) 7.
[42] H. Dau, P. Liebisch, M. Haumann, Anal. Bioanal. Chem. 376 (2003) 562.
[43] V.K. Yachandra, in: K. Sauer (Ed.), Methods in Enzymology—Biochemical Spectroscopy, Academic Press, New York, 1995, p. 638.
[44] H. Dau, M. Haumann, J. Synchrotron. Rad. 10 (2003) 76.
[45] J.E. Penner-Hahn, in: H.A.O. Hill, P.J. Sadler, A.J. Thomson (Eds.), Metal Sites in Proteins and Models: Redox Centres, Springer, Berlin, 1999, p. 1.
[46] J. Yano, J. Kern, K. Sauer, M.J. Latimer, Y. Pushkar, J. Biesiadka, B. Loll, W. Saenger, J. Messinger, A. Zouni, V.K. Yachandra, Science 314 (2006) 821.
[47] R.J. Debus, Biochim. Biophys. Acta 1503 (2001) 164.
[48] H.A. Chu, W. Hillier, N.A. Law, G.T. Babcock, Biochim. Biophys. Acta 1503 (2001) 69.
[49] T. Yamanari, Y. Kimura, N. Mizusawa, A. Ishii, T.-A. Ono, Biochemistry 43 (2004) 7479.
[50] C. Berthomieu, R. Hienerwadel, Biochim. Biophys. Acta 1707 (2005) 51.
[51] T. Noguchi, M. Sugiura, Biochemistry 39 (2000) 10943.
[52] J.M. Peloquin, R.D. Britt, Biochim. Biophys. Acta 1503 (2001) 96.
[53] G. Carrell, M. Tyryshkin, C. Dismukes, J. Biol. Inorg. Chem. 7 (2002) 2.
[54] R.D. Britt, K.A. Campbell, J.M. Peloquin, M.L. Gilchrist, C.P. Aznar, M.M. Dicus, J. Robblee, J. Messinger, Biochim. Biophys. Acta 1655 (2004) 158.
[55] P. Geijer, S. Peterson, K.A. Ahrling, Z. Deak, S. Styring, Biochim. Biophys. Acta 1503 (2001) 83.
[56] D. Koulougliotis, J.-R. Shen, N. Ioannidis, V. Petrouleas, Biochemistry 42 (2003) 3045.
[57] A. Boussac, S. Un, O. Horner, A.W. Rutherford, Biochemistry 37 (1998) 4001.
[58] J. Messinger, J.H. Nugent, M.C. Evans, Biochemistry 36 (1997) 11055.
[59] W. Hillier, T. Wydrzynski, Phys. Chem. Chem. Phys. 6 (2004) 4882.
[60] J. Messinger, M. Badger, T. Wydrzynski, Proc. Natl. Acad. Sci. U.S.A. 92 (1995) 3209.
[61] E.M. Sproviero, J.A. Gascon, J.P. McEvoy, G.W. Brudvig, V.S. Batista, J. Inorg. Biochem. 100 (2006) 786.
[62] P.E.M. Siegbahn, Quart. Rev. Biophys. 36 (2003) 91.
[63] H. Ishikita, W. Saenger, J. Biesiadka, B. Loll, E.W. Knapp, Proc. Natl. Acad. Sci. U.S.A. 103 (2006) 9855.
[64] D. Mauzerall, J.M. Hou, V.A. Boichenko, Photosynth. Res. 74 (2002) 173.
[65] M. Grabolle, H. Dau, Biochim. Biophys. Acta 1708 (2005) 209.
[66] P. Pospisil, H. Dau, Photosynth. Res. 65 (2000) 41.
[67] A.W. Rutherford, Govindjee, Y. Inoue, Proc. Natl. Acad. Sci. U.S.A. 81 (1983) 1107.
[68] J.M. Hou, V.A. Boichenko, B.A. Diner, D. Mauzerall, Biochemistry 40 (2001) 7117.
[69] H. Dau, U.P. Hansen, Photosynth. Res. 25 (1990) 269.
[70] K. Zankel, Biochim. Biophys. Acta 245 (1971) 373.
[71] Govindjee, M.P. Pulles, R. Govindjee, H.J. Van Gorkom, L.N. Duysens, Biochim. Biophys. Acta 449 (1976) 602.
[72] V.P. Shinkarev, Govindjee, Proc. Natl. Acad. Sci. U.S.A. 90 (1993) 7466.
[73] I. Vass, Photosynth. Res. 76 (2003) 303.
[74] B.G. de Grooth, H.J. van Gorkom, Biochim. Biophys. Acta 635 (1981) 445.
[75] H. Dau, U.P. Hansen, Photosynth. Res. 20 (1989) 59.
[76] J.W. Murray, J. Barber, Biochemistry 45 (2006) 4128.
[77] H. Ishikita, W. Saenger, B. Loll, J. Biesiadka, E.W. Knapp, Biochemistry 45 (2006) 2063.
[78] C.W. Hoganson, G.T. Babcock, Science 277 (1997) 1953.
[79] C.W. Hoganson, N. Lydakis-Simantiris, X.S. Tang, C. Tommos, K. Warncke, G.T. Babcock, B.A. Diner, J. McCracken, S. Styring, Photosynth. Res. 46 (1995) 177.
[80] R. Ahlbrink, M. Haumann, D. Cherepanov, O. Boegershausen, A. Mulkidjanian, W. Junge, Biochemistry 37 (1998) 1131.
[81] A.M. Hays, I.R. Vassiliev, J.H. Golbeck, R.J. Debus, Biochemistry 37 (1998) 11352.
[82] C. Zhang, S. Styring, Biochemistry 42 (2003) 8066.
[83] F. Mamedov, R.T. Sayre, S. Styring, Biochemistry 37 (1998) 14245.
[84] G. Christen, G. Renger, Biochemistry 38 (1999) 2068.
[85] F. Rappaport, J. Lavergne, Biochemistry 36 (1997) 15294.
[86] P. Joliot, A. Joliot, Biochim. Biophys. Acta 153 (1968) 635.
[87] B. Kok, B. Forbush, M. McGloin, Photochem. Photobiol. 11 (1970) 457.
[88] H. Dau, M. Haumann, Biochim. Biophys. Acta 1767 (2007) 472.
[89] J. Messinger, W.P. Schroder, G. Renger, Biochemistry 32 (1993) 7658.
[90] S. Styring, A.W. Rutherford, Biochim. Biophys. Acta 933 (1988) 378.
[91] C. Meinke, V.A. Sole, P. Pospisil, H. Dau, Biochemistry 39 (2000) 7033.
[92] M. Haumann, M. Grabolle, T. Neisius, H. Dau, FEBS Lett. 512 (2002) 116.
[93] M. Haumann, P. Pospisil, M. Grabolle, C. Muller, P. Liebisch, V.A. Sole, T. Neisius, J. Dittmer, L. Iuzzolino, H. Dau, J. Synchrotron. Rad. 9 (2002) 304.
[94] M. Haumann, C. Müller, P. Liebisch, T. Neisius, H. Dau, J. Synchrotron. Rad. 12 (2005) 35.
[95] M. Haumann, P. Liebisch, C. Müller, M. Barra, M. Grabolle, H. Dau, Science 310 (2005) 1019.
[96] H. Dau, M. Haumann, Photosynth. Res. 92 (2007) 327.
[97] H. Dau, M. Haumann, Science 312 (2006) 1471.
[98] G. Renger, Biochim. Biophys. Acta 1503 (2001) 210.
[99] M. Haumann, O. Bögershausen, D. Cherepanov, R. Ahlbrink, W. Junge, Photosynth. Res. 51 (1997) 193.
[100] G.T. Babcock, R.E. Blankenship, K. Sauer, FEBS Lett. 61 (1976) 286.
[101] M.R. Razeghifard, R.J. Pace, Biochim. Biophys. Acta 1322 (1997) 141.
[102] K.L. Westphal, N. Lydakis-Simantiris, R.I. Cukier, G.T. Babcock, Biochemistry 39 (2000) 16220.
[103] F. Rappaport, M. Blanchard-Desce, J. Lavergne, Biochim. Biophys. Acta 1184 (1994) 178.
[104] M. Haumann, W. Junge, Biochemistry 33 (1994) 864.
[105] W. Junge, M. Haumann, R. Ahlbrink, A. Mulkidjanian, J. Clausen, Phil. Trans. R. Soc. Lond., Ser. B 357 (2002) 1407.
[106] J.P. McEvoy, G.W. Brudvig, Phys. Chem. Chem. Phys. 6 (2004) 4754.
[107] J.P. McEvoy, J.A. Gascon, V.S. Batista, G.W. Brudvig, Photochem. Photobiol. Sci. 4 (2005) 940.
[108] M. Haumann, W. Junge, Biochim. Biophys. Acta 1411 (1999) 121.
[109] H.T. Witt, E. Schlodder, K. Brettel, T.M. Saygin, Photosynth. Res. 10 (1986) 453.
[110] W. Junge, in: T.W. Goodwin (Ed.), Chemistry and Biochemistry of Plant Pigments, Academic Press, London, New York, San Francisco, 1976, p. 233.
[111] J. Lavergne, Biochim. Biophys. Acta 894 (1987) 91.
[112] J.P. Dekker, J.J. Plijter, L. Ouwehand, H.J. van Gorkom, Biochim. Biophys. Acta 767 (1984) 176.
[113] G. Renger, W. Weiss, FEBS Lett. 137 (2) (1982) 217.
[114] J.P. Dekker, H.J. van Gorkom, J. Bioenerg. Biomembr. 19 (1987) 125.
[115] E. Schlodder, H.T. Witt, J. Biol. Chem. 274 (1999) 30387.
[116] J. Lavergne, W. Junge, Photosynth. Res. 38 (1993) 279.
[117] M. Haumann, W. Junge, in: Ort D., C.F. Yocum (Eds.), Oxygenic Photosynthesis: The Light Reactions, Kluwer Academic Publisher, Dordrecht, 1996, p. 165.
[118] M. Haumann, O. Boegershausen, W. Junge, FEBS Lett. 355 (1994) 101.
[119] H.T. Witt, A. Zickler, FEBS Lett. 39 (1974) 205.

[120] Saygin, H.T. Witt, FEBS Lett. 187 (2) (1985) 224.
[121] H.M. Emrich, W. Junge, H.T. Witt, Z. Naturforsch. 24 (1969) 1144.
[122] M. Haumann, A. Mulkidjanian, W. Junge, Biochemistry 36 (1997) 9304.
[123] C.F. Fowler, Biochim. Biophys. Acta 462 (1977) 414.
[124] B. Wille, J. Lavergne, Photobiochem. Photobiophys. 4 (1982) 131.
[125] S. Saphon, A.R. Crofts, Z. Naturforsch. 32C (1977) 617.
[126] P. Jahns, J. Lavergne, F. Rappaport, W. Junge, Biochim. Biophys. Acta 1057 (1991) 313.
[127] F. Rappaport, J. Lavergne, Biochemistry 30 (1991) 10004.
[128] H. Kretschmann, H.T. Witt, Biochim. Biophys. Acta 1144 (1993) 331.
[129] H. Kretschmann, E. Schlodder, H.T. Witt, Biochim. Biophys. Acta 1274 (1996) 1.
[130] G. Renger, B. Hanssum, FEBS Lett. 299 (1992) 28.
[131] A.F. Miller, G.W. Brudvig, Biochim. Biophys. Acta 1056 (1991) 1.
[132] J.C. De Paula, J.B. Innes, G.W. Brudvig, Biochemistry 24 (1985) 8114.
[133] Y. Inoue, K. Shibata, FEBS Lett. 85 (1978) 193.
[134] H.T. Witt, Ber. Bunsen Phys. Chem. 100 (1996) 1923.
[135] G. Bernat, F. Morvaridi, Y. Feyziyev, S. Styring, Biochemistry 41 (2002) 5830.
[136] M. Grabolle, Fachbereich Physik, Freie University, Berlin, http://www.diss.fu-berlin.de/2005/174/, 2005.
[137] G. Renger, G. Christen, M. Karge, H.-J. Eckert, K.-D. Irrgang, J. Biol. Inorg. Chem. 3 (1998) 360.
[138] S. Styring, A.W. Rutherford, Biochemistry 26 (1987) 2401.
[139] I. Vass, S. Styring, Biochemistry 30 (1991) 830.
[140] Z. Deak, I. Vass, S. Styring, Biochim. Biophys. Acta: Bioenerg. 1185 (1994) 65.
[141] A.W. Rutherford, Biochim. Biophys. Acta 682 (1982) 457.
[142] I. Vass, Govindjee, Photosynth. Res. 48 (1996) 117.
[143] I. Vass, Y. Inoue, in: J. Barber (Ed.), The Photosystems: Structure, Function and Molecular Biology, Elsevier, Amsterdam, 1992, p. 259.
[144] A. Szilard, L. Sass, E. Hideg, I. Vass, Photosynth. Res. 84 (2005) 15.
[145] M. Haumann, C. Muller, P. Liebisch, L. Iuzzolino, J. Dittmer, M. Grabolle, T. Neisius, W. Meyer-Klaucke, H. Dau, Biochemistry 44 (2005) 1894.
[146] J.H. Robblee, J. Messinger, R.M. Cinco, K.L. McFarlane, C. Fernandez, S.A. Pizarro, K. Sauer, V.K. Yachandra, J. Am. Chem. Soc. 124 (2002) 7459.
[147] J. Clausen, W. Junge, Nature 430 (2004) 480.
[148] J. Clausen, W. Junge, H. Dau, M. Haumann, Biochemistry 44 (2005) 12775.
[149] R.I. Cukier, D.G. Nocera, Annu. Rev. Phys. Chem. 49 (1998) 337.
[150] E. Hatcher, A. Soudackov, S. Hammes-Schiffer, Chem. Phys. 319 (2005) 93.
[151] S. Hammes-Schiffer, N. Iordanova, Biochim. Biophys. Acta: Bioenerg. 1655 (2004) 29.
[152] L.I. Krishtalik, Biochim. Biophys. Acta 1458 (2000) 6.
[153] M.R. Razeghifard, R.J. Pace, Biochemistry 38 (1999) 1252.
[154] J. Buchta, M. Grabolle, H. Dau, Biochim. Biophys. Acta 1767 (2007) 565.
[155] H. Schiller, H. Dau, J. Photochem. Photobiol. B 55 (2000) 138.
[156] F. Rappaport, M. Guergova-Kuras, P.J. Nixon, B.A. Diner, J. Lavergne, Biochemistry 41 (2002) 8518.
[157] E. Schlodder, K. Brettel, H.T. Witt, Biochim. Biophys. Acta 808 (1985) 123.
[158] C. Jeans, M.J. Schilstra, D.R. Klug, Biochemistry 41 (2002) 5015.
[159] K. Brettel, E. Schlodder, H.T. Witt, Biochim. Biophys. Acta 766 (1984) 403.
[160] M.H. Vos, H.J. van Gorkom, P.J. Van Leeuwen, Biochim. Biophys. Acta 1056 (1991) 27.
[161] L.I. Krishtalik, Biochim. Biophys. Acta 849 (1986) 162.
[162] L.I. Krishtalik, Biofizika 34 (1989) 883.
[163] L.I. Krishtalik, Biofizika 34 (1989) 1015.
[164] L.I. Krishtalik, Bioelectrochem. Bioenerg. 23 (1990) 249.
[165] H. Dau, M. Haumann, Photosynth. Res. 84 (2005) 325.
[166] J.A. Kirby, A.S. Robertson, J.P. Smith, A.C. Thompson, S.R. Cooper, M.P. Klein, J. Am. Chem. Soc. 103 (1981) 5529.
[167] V.K. Yachandra, V.J. DeRose, M.J. Latimer, I. Mukerji, K. Sauer, M.P. Klein, Science 260 (1993) 675.
[168] H. Schiller, J. Dittmer, L. Iuzzolino, W. Dörner, W. Meyer-Klaucke, V.A. Sole, H.-F. Nolting, H. Dau, Biochemistry 37 (1998) 7340.
[169] J.E. Penner-Hahn, R.M. Fronko, V.L. Pecoraro, C.F. Yocum, S.D. Betts, N.R. Bowlby, J. Am. Chem. Soc. 112 (1990) 2549.
[170] D.J. MacLachlan, B.J. Hallahan, S.V. Ruffle, J.H. Nugent, M.C. Evans, R.W. Strange, S.S. Hasnain, Biochem. J. 285 (1992) 569.
[171] V.K. Yachandra, R.D. Guiles, A. McDermott, R.D. Britt, S.L. Dexheimer, K. Sauer, M.P. Klein, Biochim. Biophys. Acta 850 (1986) 324.
[172] J. Bonvoisin, G. Blondin, J.J. Girerd, J.L. Zimmermann, Biophys. J. 61 (1992) 1076.
[173] L.V. Kulik, B. Epel, W. Lubitz, J. Messinger, J. Am. Chem. Soc. 127 (2005) 2392.
[174] K. Hasegawa, T. Ono, Y. Inoue, M. Kusunoki, Chem. Phys. Lett. 300 (1999) 9.
[175] J.M. Peloquin, K.A. Campbell, D.W. Randall, M.A. Evanchik, V.L. Pecoraro, W.H. Armstrong, R.D. Britt, J. Am. Chem. Soc. 122 (2000) 10926.
[176] T.G. Carrell, A.M. Tyryshkin, G.C. Dismukes, J. Biol. Inorg. Chem. 7 (2002) 2.
[177] M. Zheng, G.C. Dismukes, Inorg. Chem. 35 (1996) 3307.
[178] S.K. Mandal, W.H. Armstrong, Inorg. Chim. Acta 229 (1995) 261.
[179] P.A. Goodson, J. Glerup, D.J. Hodgson, K. Michelsen, E. Pedersen, Inorg. Chem. 29 (1990) 503.
[180] A. Magnuson, P. Liebisch, J. Hogblom, M.F. Anderlund, R. Lomoth, W. Meyer-Klaucke, M. Haumann, H. Dau, J. Inorg. Biochem. 100 (2006) 1234.
[181] T. Tanase, S.J. Lippard, Inorg. Chem. 34 (1995) 4682.
[182] T.K. Lal, R. Mukherjee, Inorg. Chem. 37 (1998) 2373.
[183] A.E.M. Boelrijk, S.V. Khangulov, G.C. Dismukes, Inorg. Chem. 39 (2000) 3009.
[184] I. Romero, L. Dubois, M.N. Collomb, A. Deronzier, J.M. Latour, J. Pécaut, Inorg. Chem. 41 (2002) 1795.
[185] C. Baffert, M.N. Collomb, A. Deronzier, S. Kjærgaard-Knudsen, J.M. Latour, K.H. Lund, C.J. McKenzie, M. Mortensen, L. Nielsen, N. Thorup, Dalton Trans. (2003) 1765.
[186] H.H. Thorp, J.E. Sarneski, G.W. Brudvig, R.H. Crabtree, J. Am. Chem. Soc. 111 (1989) 9249.
[187] E.J. Larson, V.L. Pecoraro, in: V.L. Pecoraro (Ed.), Manganese Redox Enzymes, VCH Publishers, New York, 1992.
[188] M.J. Baldwin, N.A. Law, T.L. Stemmler, J.W. Kampf, J.E. Penner-Hahn, V.L. Pecoraro, Inorg. Chem. 38 (1999) 4801.
[189] R. Manchanda, H.H. Thorp, G.W. Brudvig, R.H. Crabtree, Inorg. Chem. 30 (1991) 494.
[190] R. Manchanda, H.H. Thorp, G.W. Brudvig, R.H. Crabtree, Inorg. Chem. 31 (1992) 4040.
[191] M.J. Baldwin, V.L. Pecoraro, J. Am. Chem. Soc. 118 (1996) 11325.
[192] M.T. Caudle, V.L. Pecoraro, J. Am. Chem. Soc. 119 (1997) 3415.
[193] J.E. Penner-Hahn, Coord. Chem. Rev. 190–192 (1999) 1101.
[194] B. Teo, EXAFS: Basic Principles and Data Analysis, Springer-Verlag, Berlin, Germany, 1986.
[195] D.C. Koningsberger, B.L. Mojet, G.E. van Dorssen, D.E. Ramaker, Topics Catal. 10 (2000) 143.
[196] V.K. Yachandra, Phil. Trans. R. Soc. Lond. B: Biol. Sci. 357 (2002) 1347 (Discussion 1357–1358, 1367).
[197] V.K. Yachandra, K. Sauer, M.P. Klein, Chem. Rev. 96 (1996) 2927.
[198] J.E. Penner-Hahn, in: J.A. McCleverty, T.J. Meyer (Eds.), Comprehensive Coordination Chemistry, vol. II, Elsevier Ltd., Oxford, UK, 2004, p. 159.
[199] J.E. Penner-Hahn, Structure and Bonding: Metal Sites in Proteins and Models: Redox Centres, Springer-Verlag, Heidelberg, Germany, 1998, pp. 1–36.
[200] H. Dau, J. Dittmer, L. Iuzzolino, H. Schiller, W. Dörner, I. Heinze, V.A. Sole, H.-F. Nolting, J. Phys. IV 7 (1997) 607.
[201] R.B.G. Ravelli, S.M. McSweeney, Structure 8 (2000) 315.
[202] R.B.G. Ravelli, P. Theveneau, S. McSweeney, M. Caffrey, J. Synchrotron. Rad. 9 (2002) 355.
[203] H. Dau, J.C. Andrews, T.A. Roelofs, M.J. Latimer, W. Liang, V.K. Yachandra, K. Sauer, M.P. Klein, Biochemistry 34 (1995) 5274.
[204] M. Haumann, M. Grabolle, M. Werthammer, L. Iuzzolino, J. Dittmer, W. Meyer-Klaucke, T. Neisius, H. Dau, Proceedings of the 12th International

Congress of Photosynthesis, CSIRO Publishing, Melbourne, Australia, 2001, pp. 1–5.
[205] J. Dasgupta, R.T. van Willigen, G.C. Dismukes, Phys. Chem. Chem. Phys. 6 (2004) 4793.
[206] E.M. Sproviero, J.A. Gascon, J.P. McEvoy, G.W. Brudvig, V.S. Batista, Curr. Opin. Struct. Biol. 17 (2007) 173.
[207] J.E. Penner-Hahn, in: H.A.O. Hill, A. Thomson (Eds.), Metal Sites in Proteins and Models, Springer-Verlag, Heidelberg, 1999, p. 1.
[208] G.N. George, R.C. Prince, S.P. Cramer, Science 243 (1989) 789.
[209] I. Mukerji, J.C. Andrews, V.J. DeRose, M.J. Latimer, V.K. Yachandra, K. Sauer, M.P. Klein, Biochemistry 33 (1994) 9712.
[210] H. Dau, A. Grundmeier, P. Loja, M. Haumann, Phil. Trans. R. Soc. Lond., Ser. B, in press.
[211] G.C. Dismukes, Y. Siderer, Proc. Natl. Acad. Sci. U.S.A. 78 (1981) 274.
[212] D. Kuzek, R.J. Pace, Biochim. Biophys. Acta (BBA)—Bioenerg. 1503 (2001) 123.
[213] P.J. Riggs-Gelasco, R. Mei, J.E. Penner-Hahn, in: Advances in Chemistry Series, vol. 246, Society, A.C., 1995, pp. 219–248.
[214] P. Glatzel, U. Bergmann, J. Yano, H. Visser, J.H. Robblee, W. Gu, F.M. de Groot, G. Christou, V.L. Pecoraro, S.P. Cramer, V.K. Yachandra, J. Am. Chem. Soc. 126 (2004) 9946.
[215] T. Ono, T. Noguchi, Y. Inoue, M. Kusunoki, T. Matsushita, H. Oyanagi, Science 258 (1992) 1335.
[216] L. Iuzzolino, J. Dittmer, W. Dörner, W. Meyer-Klaucke, H. Dau, Biochemistry 37 (1998) 17112.
[217] T.A. Roelofs, W. Liang, M.J. Latimer, R.M. Cinco, A. Rompel, J.C. Andrews, K. Sauer, V.K. Yachandra, M.P. Klein, Proc. Natl. Acad. Sci. U.S.A. 93 (1996) 3335.
[218] J. Messinger, J.H. Robblee, U. Bergmann, C. Fernandez, P. Glatzel, H. Visser, R.M. Cinco, K.L. McFarlane, E. Bellacchio, S.A. Pizarro, S.P. Cramer, K. Sauer, M.P. Klein, V.K. Yachandra, J. Am. Chem. Soc. 123 (2001) 7804.
[219] H. Dau, P. Liebisch, M. Haumann, Phys. Scripta T115 (2005) 844.
[220] H. Dau, L. Iuzzolino, J. Dittmer, W. Dörner, W. Meyer-Klaucke, in: G. Garab (Ed.), Photosynthesis: Mechanisms and Effects, Kluwer Academic Publishers, Dordrecht, 1998, p. 1327.
[221] P. Liebisch, Thesis, Physics Department, Freie Universität Berlin, Berlin, 2005.
[222] J. Messinger, J. Robblee, W.O. Yu, K. Sauer, V.K. Yachandra, M.P. Klein, J. Am. Chem. Soc. 119 (1997) 11349.
[223] K.A. Åhrling, S. Peterson, S. Styring, Biochemistry 36 (1997) 13148.
[224] E.J. Larson, P.J. Riggs, J.E. Penner-Hahn, V.L. Pecoraro, J. Chem. Soc. Chem. Commun. (1992) 102.
[225] V.K. Yachandra, R.D. Guiles, A.E. McDermott, J.L. Cole, R.D. Britt, S.L. Dexheimer, K. Sauer, M.P. Klein, Biochemistry 26 (1987) 5974.
[226] A. Boussac, J.L. Zimmermann, A.W. Rutherford, J. Lavergne, Nature 347 (1990) 303.
[227] B.J. Hallahan, J.H. Nugent, J.T. Warden, M.C. Evans, Biochemistry 31 (1992) 4562.
[228] P.E.M. Siegbahn, Curr. Opin. Chem. Biol. 6 (2002) 227.
[229] I.D. Brown, D. Altermatt, Acta Crystallogr. Sect. B 41 (1985) 244.
[230] V.S. Urusov, Acta Crystallogr. Sect. B 51 (1995) 641.
[231] N.E. Brese, M. O'Keeffe, Acta Crystallogr. Sect. B 47 (1991) 192.
[232] A.L. Ankudinov, B. Ravel, J.J. Rehr, S.D. Conradson, Phys. Rev. B 12 (1998) 7565.
[233] P.E.M. Siegbahn, Inorg. Chem. 39 (2000) 2923.
[234] P.E.M. Siegbahn, R.H. Crabtree, J. Am. Chem. Soc. 121 (1999) 117.
[235] W. Liang, T.A. Roelofs, R.M. Cinco, A. Rompel, M.J. Latimer, W.O. Yu, K. Sauer, M.P. Klein, V.K. Yachandra, J. Am. Chem. Soc. 122 (2000) 3399.
[236] G. Hendry, T. Wydrzynski, Biochemistry 41 (2002) 13328.
[237] W. Hillier, J. Messinger, T. Wydrzynski, Biochemistry 37 (1998) 16908.
[238] W. Hillier, T. Wydrzynski, Biochemistry 39 (2000) 4399.
[239] C.C. Moser, J.M. Keske, K. Warncke, R.S. Farid, P.L. Dutton, Nature 355 (1992) 796.
[240] H. Frauenfelder, P.G. Wolynes, Science 229 (1985) 337.
[241] H. Frauenfelder, S.G. Sligar, P.G. Wolynes, Science 254 (1991) 1598.
[242] H. Frauenfelder, B.H. McMahon, R.H. Austin, K. Chu, J.T. Groves, Proc. Natl. Acad. Sci. U.S.A. 98 (2001) 2370.
[243] J.M. Kriegl, G.U. Nienhaus, Proc. Natl. Acad. Sci. U.S.A. 101 (2004) 123.
[244] S. Hammes-Schiffer, S.J. Benkovic, Annu. Rev. Biochem. 75 (2006) 519.
[245] K.F. Wong, T. Selzer, S.J. Benkovic, S. Hammes-Schiffer, Proc. Natl. Acad. Sci. U.S.A. 102 (2005) 6807.
[246] A. Boussac, F. Rappaport, P. Carrier, J.M. Verbavatz, R. Gobin, D. Kirilovsky, A.W. Rutherford, M. Sugiura, J. Biol. Chem. 279 (2004) 22809.
[247] G. Hendry, T. Wydrzynski, Biochemistry 42 (2003) 6209.
[248] W. Hillier, G. Hendry, R.L. Burnap, T. Wydrzynski, J. Biol. Chem. 276 (2001) 46917.
[249] R. Tagore, H. Chen, R.H. Crabtree, G.W. Brudvig, J. Am. Chem. Soc. 128 (2006) 9457.
[250] N. Ioannidis, V. Petrouleas, Biochemistry 41 (2002) 9580.
[251] N. Ioannidis, J.H.A. Nugent, V. Petrouleas, Biochemistry 41 (2002) 9589.